WILEY | Hindawi

Review Article

A Review of Membrane Electrode Assemblies for the Anion Exchange Membrane Water Electrolyser: Perspective on Activity and Stability

T. B. Ferriday (ID),[1,2] **S. N. Sampathkumar** (ID),[2] **P. H. Middleton** (ID),[1,2] **M. L. Kolhe** (ID),[1] **and J. Van Herle** (ID)[2]

[1]*Department of Engineering Science, University of Agder, Jon Lilletuns vei 9, Grimstad 4879, Agder, Norway*
[2]*Group of Energy Materials, Swiss Federal Institute of Technology, Lausanne, Rue de l'Industrie 17, Sion 1951, Valais, Switzerland*

Correspondence should be addressed to T. B. Ferriday; thomasbferriday@gmail.com

The performance of a water electrolyser (WE) depends on several aspects, many of which are located in the powerhouse of the cell, namely, the membrane electrode assembly (MEA). The anion exchange membrane WE (AEMWE) is a promising technology; however, both activity and stability must be further developed to surpass the current dominant WE technologies. Herein, we review aspects related to MEA development for anion exchange membrane water electrolysers, covering materials and techniques from the perspective of stability and activity. The gas diffusion layer (GDL) and the microporous layer (MPL) are often combined into a single MEA component, which places great importance on its composition. This composite layer has the greatest impact of any single component on cell performance, as the physical architecture of the GDL/MPL influences the overpotential related to activation, ohmic, and mass transport. The purpose of this review is to serve as an executive summary of the literature related to MEAs for AEMWEs for researchers and industry professionals who seek to further the state of the art.

1. Introduction

The production of green hydrogen has gained traction in recent years as the world enters a transition period to minimise fossil fuel consumption. Hydrogen is an intermediate energy vector, of which about 95% is produced by reforming methane and coal [1–6]. The fluctuations in renewable energy sources, such as wind energy and solar photovoltaic production, allow the implementation of green hydrogen production technology as an energy conversion device. The most prominent method for producing green hydrogen has been water electrolysis. The technologies that dominate water electrolysis include the traditional liquid alkaline water electrolyser (AWE) and the proton exchange membrane water electrolyser (PEMWE). PEMWE uses a deionised water liquid electrolyte that becomes acidic during operation, thus requiring expensive platinum group metal (PGM) catalysts, such as Pt, Ir, Ru, and various bimetallic combinations and oxides, namely PtRu and IrO_2. PEMWEs

can operate with high current densities ($j \geq 3.0 \, A \, cm^{-2}$) and rapid system dynamics, allowing load-following operations [7]. AWE systems operate under high pH conditions, allowing the use of non-PGM metals such as Ni, Fe, and Mo, although at a significantly lower current density ($j \approx 0.50 \, A \, cm^{-2}$) due to slower kinetics and greater ohmic resistance.

The classical AWE system was improved with the development of zero-gap technology, which reduced the ohmic resistance, although the current density is still considerably lower than that achieved with PEMWEs. Other remaining issues include the highly corrosive electrolyte (45 wt.% KOH $\approx 8.0 \, M$ KOH), a more complicated system design and a lower purity of hydrogen [1–5]. The anion exchange membrane (AEM) solves several of these problems and acts as an alkaline version of PEMWE, where it combines the advantages of the PEMWE and AWE system by using non-PGM electrocatalysts, low-alkali electrolytes (pH 7-12) and incorporating the possibility of electrochemical hydrogen compression (up to 30 bar) as highlighted in Table 1

TABLE 1: Comparison of the three main low-temperature electrolyser technologies.

Electrolyser →	AEMWE	PEMWE	AWE
Circulating electrolyte	0.1-1.0 M KOH [18, 19]	Deionised water [7]	4.5-8.0 M KOH [18, 19]
Current density (A cm^{-2})	1-2 [18, 19]	1-3 [7, 19]	0.2-0.8 [19]
Cell voltage (V)	1.4-2.0 [18, 19, 20]	1.4-2.3 [7, 21]	1.4-3.0 [19]
Temperature (°C)	60-80 [18, 19]	50-90 [7]	80-120 [22]
Anode (OER)	NiFeO$_x$ [22]	IrO$_2$ [7, 22]	Ni, Ni-Co [22]
Cathode (HER)	NiCo [22]	Pt/C [7, 22]	Ni, Ni-Mo [22]
Efficiency (LHV%)	52-75 [19, 23]	50-68 [19]	50-68 [19]
Maturity	kW—small commercial units	MW—large commercial units	MW—mature
Stack life (yr)	>5000 [19]	20 000-90 000	>90 000
Cost (stack) (€ kW^{-1})	320-1000 (1-10 MW)* [24, 25]	360-900 (1-10 MW)* [19, 25]	240-600 (1-10 MW)* [19, 25]
Degradation rate (μV h^{-1})	5-1000 [18]	5-200 [26, 27]	5-20 [28, 29]

*Some of these values have been calculated to euros based of 1 USD ≈0.91 EUR.

[8, 9]. The working principle of the electrolyser system is summarised in Figure 1.

The state-of-the-art AEMWE single cell should consist of a membrane with an ionic conductivity ≥80 S cm^{-1} in 1.0 M KOH at 30°C [10], sandwiched between a non-PGM HER and OER electrocatalyst, performing at 10 mA cm^{-2} with overpotentials of less than 100 mV and 300 mV including iR-correction, respectively [11].

The current state-of-the art non-PGM AEMWE performance (iR corrected) is 1.0 A cm^{-2} at 1.57 V with a Fe-NiMo-NH$_3$/H$_2$||NiMo-NH$_3$/H$_2$ anode||cathode in 1.0 M KOH at 80°C, employing a Sustainion® X37-50 T AEM [11]. Other admirable performances include reaching 1.0 A cm^{-2} at 1.63 V with IrO$_2$||Pt/C anode||cathode in 1.0 M KOH, 60°C with the same Sustainion® membrane [12]. Ding et al. [13] achieved a current density of 1.0 A cm^{-2} at 1.65 V (iR corrected) with a Ni$_2$Fe$_8$–Ni$_3$S$_2$/NF||Ni$_4$Mo/MoO$_2$/NF anode||cathode in 1.0 M KOH at 80°C also using a Sustainion® AEM. In little contrast, PEMWEs reach 1.0 A cm^{-2} at 1.56 V with a IrO$_2$||Pt/C anode||cathode at 90°C [14, 15].

The longest durability test reported using AEMWEs is around 12000 hours [15, 16] at 1.0 A cm^{-2}, 60°C, and 1.0 M KOH, with a voltage degradation rate of 0.7 μV h^{-1}. Here, the Sustainion® X37-50 T AEM was utilised with NiFe$_2$O$_4$ (1.8 mg cm^{-2}) on nickel fibre and Raney® Ni (14.5 mg cm^{-2}) as the anode/cathode catalyst. The longest durability test facilitated in pure water lasted 2200 hours, conducted at 0.2 A cm^{-2} at 50°C, which produced a degradation rate of 0.2 mV h^{-1} [17]. The IrO$_2$||Pt anode/cathodes degraded rapidly due to durability issues associated with the stability of the AEM/ionomer under neutral conditions. For comparison, the durability of PEMWEs varies, though commercial systems are expected to operate for 60.000 hours with negligible degradation, and experimental degradation rates are reported in the range of 5 μV h^{-1} [14].

To advance these performances, the membrane electrode assembly (MEA) must be optimised. Furthermore, this is also the principal way to advance the state of the art for AEMWEs, as the end goal is to replace PEMWEs with a more cost-effective solution that exhibits comparable activity and durability. However, creating a perfect MEA is not easy.
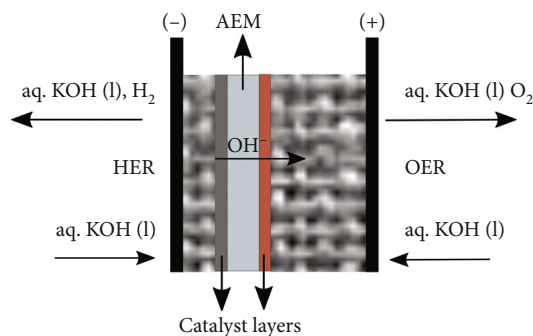

FIGURE 1: Simple schematic of an AEM water electrolyser.

The MEA is the most complicated and interlaced facet of the AEMWE, both figuratively and literally. Several layers are combined to create the MEA, each performing different tasks to ensure a stable flow of reactants and products to and from the triple-phase interface, between the catalyst layer and the AEM. It is also responsible for maintaining the electrical conductivity from the polarised flow fields to the catalyst layers, enabling the imposed electrical potential to overcome the thermodynamic barrier to incite the electrochemical reactions.

Most challenges at the single-cell level lie within the MEA, where this facet sequentially comprises the gas diffusion layer (GDL), the microporous layer (MPL), the catalyst layer (CL), and, finally, the membrane as illustrated in Figure 2. Each of these components has specific roles related to the transport of reactant, product, ions, and electrons. However, the optimal transport of these elements involves a trade-off, because efficient transportation of fluids requires volume and space, whereas that of charge is aided by high conductivity produced by a lack of volume and space. That is, increasing one will decrease the other. The ideal MEA balances the transport of fluid and charge, and although one cannot avoid this conundrum, the side effects can be reduced, as will be shown throughout this review.

While the roles of each component are usually firmly divided for offhand explanations, the reality is that their
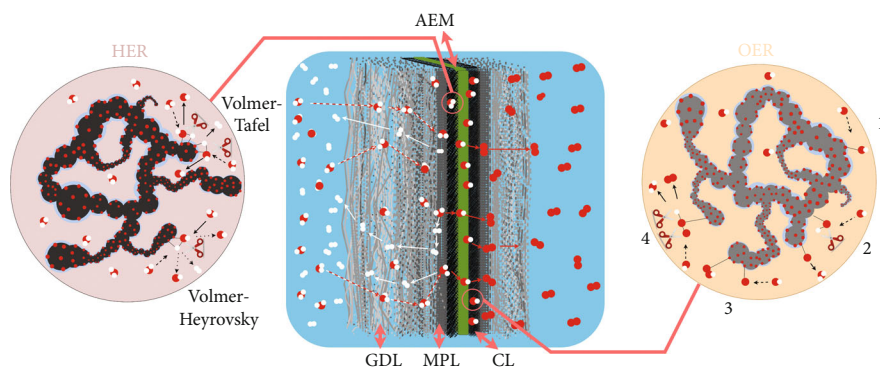
FIGURE 2: Detailed illustration of the MEA. The water reactant on the cathode side (left) is reduced to produce hydrogen and the hydroxide anion charge carrier, which diffuses through the AEM to be oxidised in the oxygen evolution reaction to produce oxygen gas and water. The cathodic hydrogen evolution reaction (HER) (left), where each step is also illustrated. HER will occur through either the Volmer-Tafel or Volmer-Heyrovsky pathway. Briefly, the catalyst will adsorb a water molecule and sever an OH-H bond leaving only an adsorbed H atom (Volmer step), and provided the same occurring on a neighbouring site, the two may combine to form molecular hydrogen (Tafel). The second option is where another water molecule reacts with an adsorbed H atom to form a hydroxide charge carrier and molecular hydrogen (Heyrovsky). The anodic oxygen evolution reaction (OER) is also shown (right). Briefly, a hydroxide anion is adsorbed onto an active site (1), after which another such anion reacts with the adsorbed species to form water, leaving an adsorbed O atom (2). Hydroxide interacts with the adsorbed O atom to form adsorbed OOH (3), before another OH^- anion reacts with this adsorbate to form oxygen gas and water (4).

roles are rather interlaced. The simplified version is that the gas diffusion layer (GDL) (Figure 2) provides a highly porous pathway for two-phase flow from the flow fields into the MPL, while transferring electrical charge and heat. The GDL also helps to uniformly distribute pressure across the rest of the MEA, which is crucial for cell health, as irregularity causes uneven depreciation and accelerated cell ageing. The MPL has pathways considerably smaller than those of the GDL, which provides a large electrochemical surface area and good electrical contact towards the side facing the membrane, which is covered with the CL. The CL takes advantage of the large surface area offered by the MPL over which a great number of catalytic sites are distributed. Catalysis occurs by lowering the total energy necessary to facilitate the transition from reactant to product, which proceeds continuously on each site in the triple-phase boundary, composed of catalyst/ionomer, electrolyte reactant, and gaseous product. This allows the reaction to be energetically feasible.

Each part of the MEA will now be reviewed from the perspective of conductivity and fluid dynamics with respect to the GDL and MPL. The CL will also cover these aspects, although greater emphasis is placed on the materials involved and how they affected stability and performance. Finally, the topic of MEA preparation will also be examined, since it can also have a fair effect on the resulting stability and performance.

2. Gas Diffusion Layer

The gas diffusion layer is a component of many names, sometimes referred to as a porous transport layer (PTL), a current collector, or a liquid-gas diffusion layer (LGDL) [30]. This is the primary recipient of the electrolyte from the flow field and the final MEA component to handle the product gases, which means that maintaining efficient fluid dynamics is one of its core tasks. Similar aspects are also handled by the MPL, resulting in many electing to use a single component to act as both GDL and MPL. This is achieved by placing the CL directly on top of the GDL [31–40], placing even greater significance on the GDL design. Moreover, the GDL has been highlighted as the single most influential component in the MEA through a recent statistical study comparing the importance of the type of GDL, the type of catalyst, the catalyst loading and the amount of additive carbon [41]. There are several commercial GDL alternatives such as Sigracet and Toray [42]; however, considering its importance, there are many experimental GDL varieties in which aspects such as fluid dynamics and interfacial contact resistance (ICR) have been optimised.

Many current GDL designs originate from PEM technology, as the similarities between PEM and AEM technology render much of the know-how highly transferable. Beneficially, this is possible without transferring the pesky electrochemical conditions associated with the PEMWE anode, which requires expensive titanium to handle its highly corrosive acidic environment [30]. Inexpensive nickel foam can be used freely as a GDL in AEMWEs on both the anode and the cathode side and is the most widely used GDL material for AEMWEs [43].

The GDL is the layer closest to the flow field of the AEMWE, and thus, its properties relative to fluid dynamics often take centre stage when evaluating materials. However, it is also the first point of contact for the charge passing through an electrically conductive flow field. This equalises the importance of aspects related to both fluid dynamics and charge transfer [31]. Considering the significance of reducing the ohmic resistance, we will first consider the conductivity.

(a)   (b)
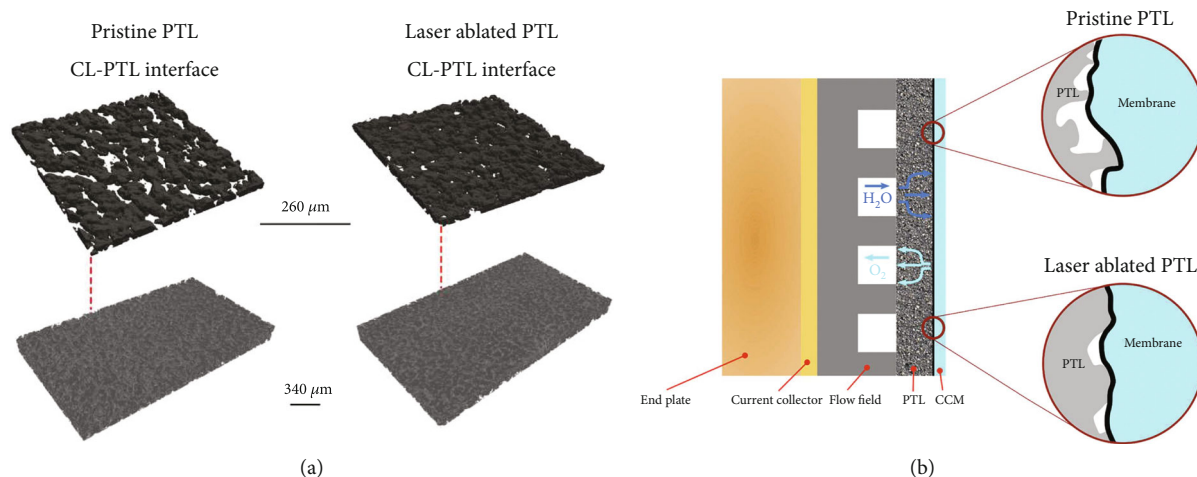
FIGURE 3: (a) X-ray computed tomographic figures of pristine and laser-ablated GDLs (referred to as PTLs in the figure text) and (b) the resulting improvement in the GDL/CL/AEM interface [46].

2.1. GDL: The Conductivity. The importance of conductivity through anodic and cathodic GDL/MPL is identical, and this aspect is optimised through the same processes for either electrode. As such, the treatments introduced may be considered equally effective for both the anode and the cathode, with respect to conductivity. The conductivity of the GDL depends on both the intrinsic electrical resistivity of the materials involved and the interfacial contact resistance (ICR) at the flow field|GDL|MPL interfaces [44].

Plasma air spraying of nickel powder reduced the ICR by 75% for a stainless steel GDL, resulting in a combined GDL-MPL [44]. This contributed to a 290 mV reduction in overpotential compared to untreated GDLs, based on subsequent LSV curves from a single-cell AEMWE. Similar conclusions were reached in a comparison between nickel felt and nickel foam, where the uneven surface and the high porosity of the latter increased ICR, making nickel felt the superior choice [45]. However, mitigating these issues through simple surface modifications such as sanding down the foam surface or choosing a grade with lower porosity has also been shown to be effective. Such simple steps can be fruitful, as there are great variations in nickel foam with respect to both porosity (density of nickel structure) and conductivity (thickness of nickel strands). Another way of modifying the surface is by cutting various patterns with a laser, where the laser polishes the rough morphology of the nickel foam while the untouched foam retains its imperfections [46]. This enhanced the GDL-CL contact (Figure 3) and reduced both series resistance and charge transfer resistance during water electrolysis. However, overzealous laser use resulted in dead-ended pores, ultimately exacerbating potential mass transportation issues.

Considering activation overpotential is the first limitation, any reduction thereof will improve electrolyser performance regardless of whether the cell is operated at normal (1.0-2.0 A cm^{-2}) or high current densities (>5.0 A cm^{-2}). Laser ablation modified the surface of titanium GDLs, creating structures reminiscent of an MPL which naturally improved surface contact, increased catalyst utilisation, and enhanced electrolyte performance [46]. This illustrates that adding MPL qualities to a GDL can reduce MEA complexity and increase efficiency [46]. However, it should be emphasised that nickel is usually preferred over titanium due to improved stability and lower financial cost [31, 41]. This was explicitly shown in a comparative study of GDL materials featuring titanium felt, nickel felt, and nickel foam as displayed in Figure 4(a) [31].

A switch from titanium to nickel unveiled a ×50 reduction in electrical sheet resistance, and the difference in performance between titanium and nickel GDLs in an alkaline electrolyte is stark, as shown in Figures 4(b)–4(d). Moreover, it is clear from these figures that the use of titanium is not easy, as it can easily passivate by forming a protective, insulating oxide layer, which increases its electrical resistance. Furthermore, crevice corrosion can occur during industrially relevant operating conditions ($E \leq 2.0$ V, $j \geq 1.0$ A cm^{-2}, $T \geq 50°C$), which impedes long-term stability [47].

Grid architectures for GDLs have also been investigated, where the overall performance of 3D-printed nickel grid GDLs did not increase continuously as the size of the grid increased [48]. Specifically, a volcano-relationship was determined, peaking at 240 μm. This was explained by issues such as large ICRs and low catalyst utilisation, two issues that plague overly porous GDLs [45, 48].

Manipulating the pore size distribution throughout the thickness of the GDL was utilised as a means of improving the flow of both charge and fluid. Varying the size of the titanium particles used during vacuum plasma spraying onto mild steel produced a gradient in pore size along the thickness of the GDL (large porse towards the flow field, smaller pores towards the CL), which improved both electrical contact with the flow field and facilitation of the two-phase flow [34].

The surface structure and pore size for stainless steel GDLs were varied, and the highest AEMWE performance was achieved with the fine-fibre SS10 GDL, representing a 100 mV reduction in ohmic overpotentials compared to the coarser SS100 GDL [49]. As such, electrical contact between the flow field and the GDL is of great importance. This becomes clear when a CL is applied on top of the GDL, as
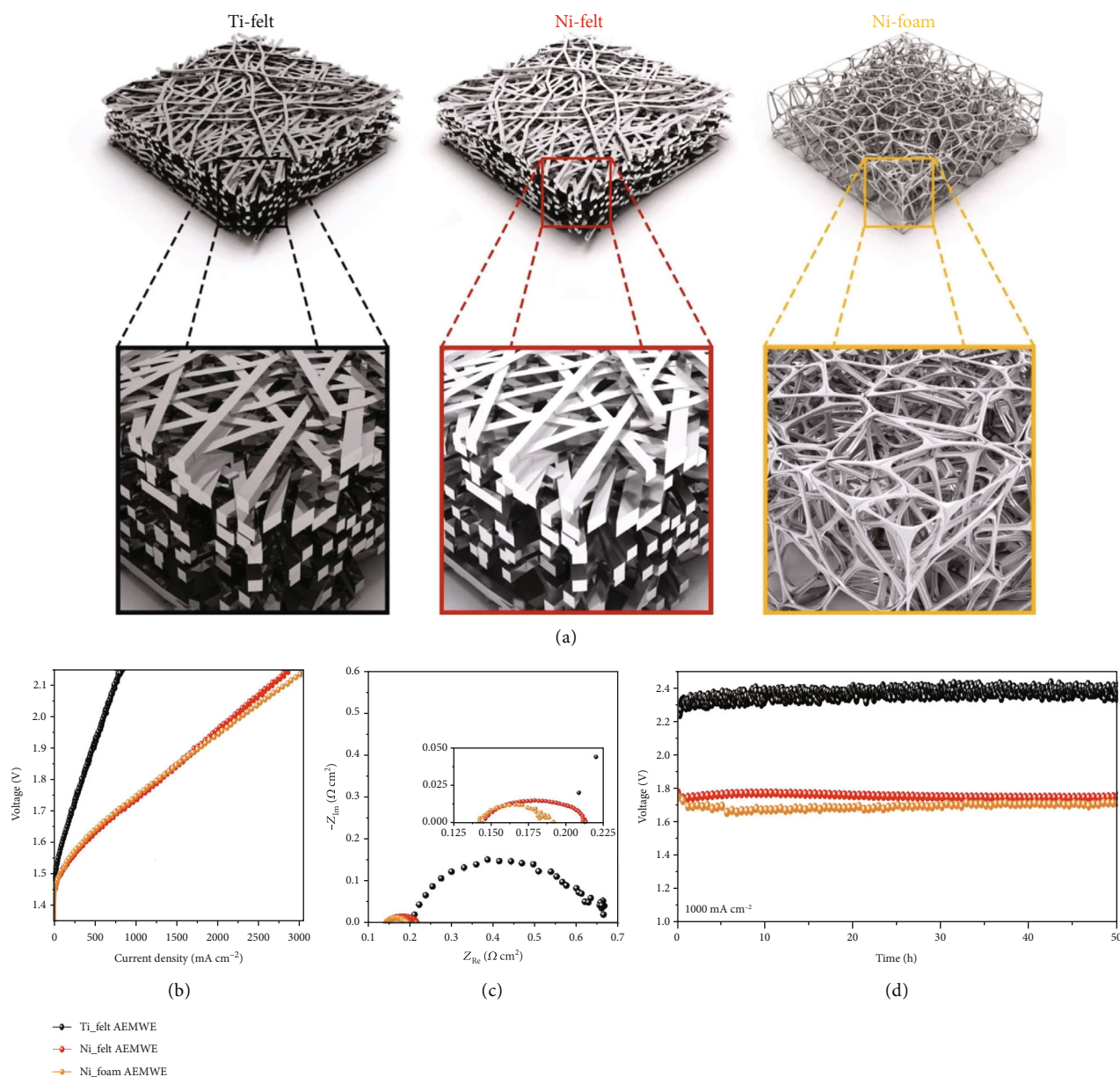
Figure 4: (a) Visualisation of three different GDL materials. (b) LSV curves and (c) EIS spectra of AEMWEs utilising the different GDLs in 1.0 M KOH at 70°C. (d) Chronopotentiometry of the three AEMWEs at 1.0 A cm^{-2} in 1.0 M KOH at 70°C. Reprinted with permission from [31]. Copyright 2023 John Wiley and Sons.

the overzealous use of, e.g., PTFE in the CL will decrease its conductivity while increasing its mechanical stability and hydrophobicity, the latter of which is beneficial for water management.

2.2. GDL: Fluid Dynamics.

Fluid dynamics play an important part in MEAs, as a great current density will require an equally great fluid flow to supply reactants and aid in dispelling products. Insufficient fluid dynamics may induce notable mass transport (MT) overpotential; however, industrial electrolysis systems are usually operated in a potential region dominated by kinetic and ohmic overpotential. The potential at which the effects of MT are noticeable will vary between different water electrolyser systems, and they

should not play a significant role under industrially relevant conditions ($E \leq 2.0$ V, $j \geq 1.0$ A cm^{-2}, $T \geq 50°C$). Therefore, it is sufficient for GDLs to handle fluid flows associated with such conditions, where the design of GDLs that can handle high current densities ($j \geq 5.0$ A cm^{-2}) can negatively impact the ohmic overpotential.

The GDL thickness was systematically varied for the anode (250 μm, 350 μm, and 400 μm) and the cathode (270 μm, 320 μm, and 420 μm) [50], where the optimal GDL anode thickness was 350 μm using a Ti-GDL (with a 250 μm gasket) together with a 420 μm carbon GDL on the cathode. The 350 μm Ti-GDL outperformed the others due to a trade-off between ICR and MT overpotential. The AEMWE performance improved continuously as the
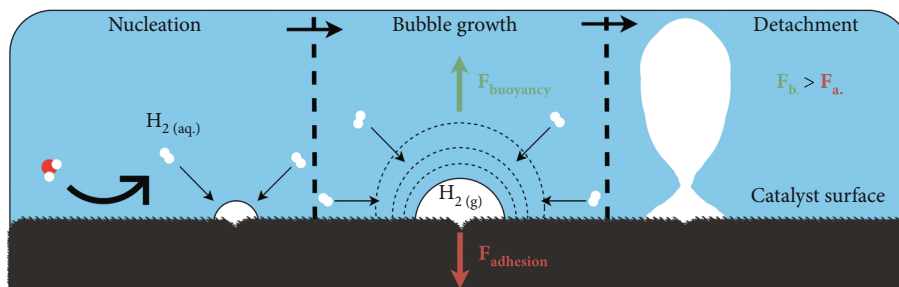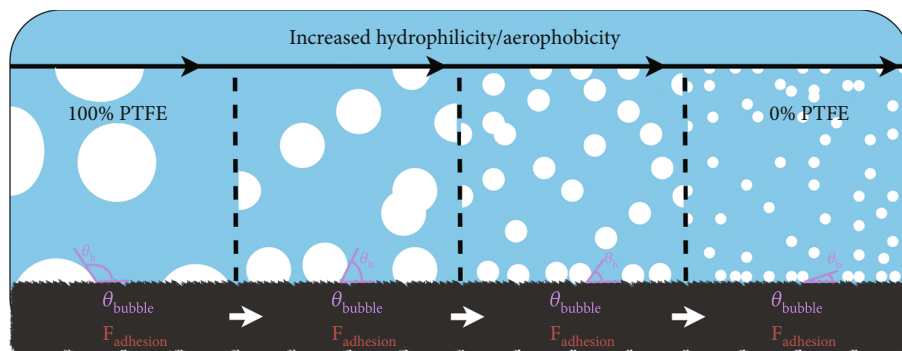
FIGURE 5: Bubble creation process [55].

FIGURE 6: Change in bubble dynamics through changes to the surface hydrophilicity/aerophobicity.

cathode GDL thickness increased; thus, a peak performance was achieved with the $420\,\mu m$ carbon GDL (with a $350\,\mu m$ anode Ti-GDL) due to improved ICR.

Water is present as a product on the anode while it is a reactant on the cathode, which means that fluid dynamics play an important role on both electrodes. There is some uncertainty in the literature on which of the two has the greatest impact with respect to fluid dynamics, where some claim the anode [51], while others claim the same for the cathode [52]. However, a greater emphasis is generally placed on investigating the anodic fluid dynamics [31, 48, 51]. This imbalance occurs despite the similarity between the bubble sizes of hydrogen and oxygen gas [53], and that the cathode will produce twice as much gas as the anode based off stoichiometry. This section primarily details the anode GDL. There are several reports detailing the benefits of operating with a dry cathode, though this will be discussed later in subsection 4.3.

Typically, there are two phases in the fluid flow in GDLs, implying that handling both liquid and gas is relevant. To this effect, handling bubble growth is important and is a continuous process that begins when the dispersed gases reach the supersaturation point, as exhibited in Figure 5. Bubbles will typically nucleate in the GDL at the triple phase boundary point and detach once a critical size has been reached for CL-coated GDLs [54].

This size can be altered by increasing the hydrophilicity and aerophobicity of the surface, which will reduce the contact surface of the GDL bubble, thus decreasing the contact angle of the gas bubble and ultimately lowering the adhesion force between the bubble and the surface [56]. This allows bubbles to rapidly detach and increases the product flow

rate, as illustrated in Figure 6. Nickel GDLs produced through 3D printing had this effect, which reduced overpotentials related to activation, ohmic, and mass transportation in an AEMWE with deionised water as the liquid electrolyte. MT overpotential was reduced by 84.9% and 86.1% at 0.5 and $1.0\,A\,cm^{-2}$ relative to traditional nickel foam. This drastic improvement in fluid handling contributed to lowering the overpotential by $71\,mV$ at $2.0\,A\,cm^{-2}$ [56].

The effects of modifying the surface hydrophobicity have been investigated by varying the anode surface coverage of polytetrafluoroethylene (PTFE) during coelectrodeposition of nickel and PTFE [57]. The electrodes beheld a notable variety of PTFE coverage (0, 0.17, 0.55, 0.76), causing equally notable changes in oxygen bubble evolution. The departure diameter of the bubbles increased significantly when the surface coverage of PTFE increased from 0.17 to 0.55-0.76. This was attributed to an increase in contact angle and bubble adhesion force, resulting from smaller bubbles coalescing until the buoyancy force exceeded the adhesion force, causing bubble detachment, as shown in Figures 5 and 6. A design parameter was identified, where the ratio of the bubble departure diameter to the GDL pore diameter should be less than unity $((d_{\text{bubble,dep.}}/d_{\text{pore}}) < 1)$ for an electrode to avoid notable issues related to the MT overpotential induced by gas bubble accumulation.

Gas evolution is efficiently handled in three-dimensional networks, as demonstrated by comparing nickel foams and felts as anode GDLs. Here, the former was preferred due to its three-dimensional interconnected pores, which helped reduce ohmic resistance while maintaining rapid gas/liquid flow [36]. Comparatively, nickel felt has only fully developed pores in the direction perpendicular to the membrane,
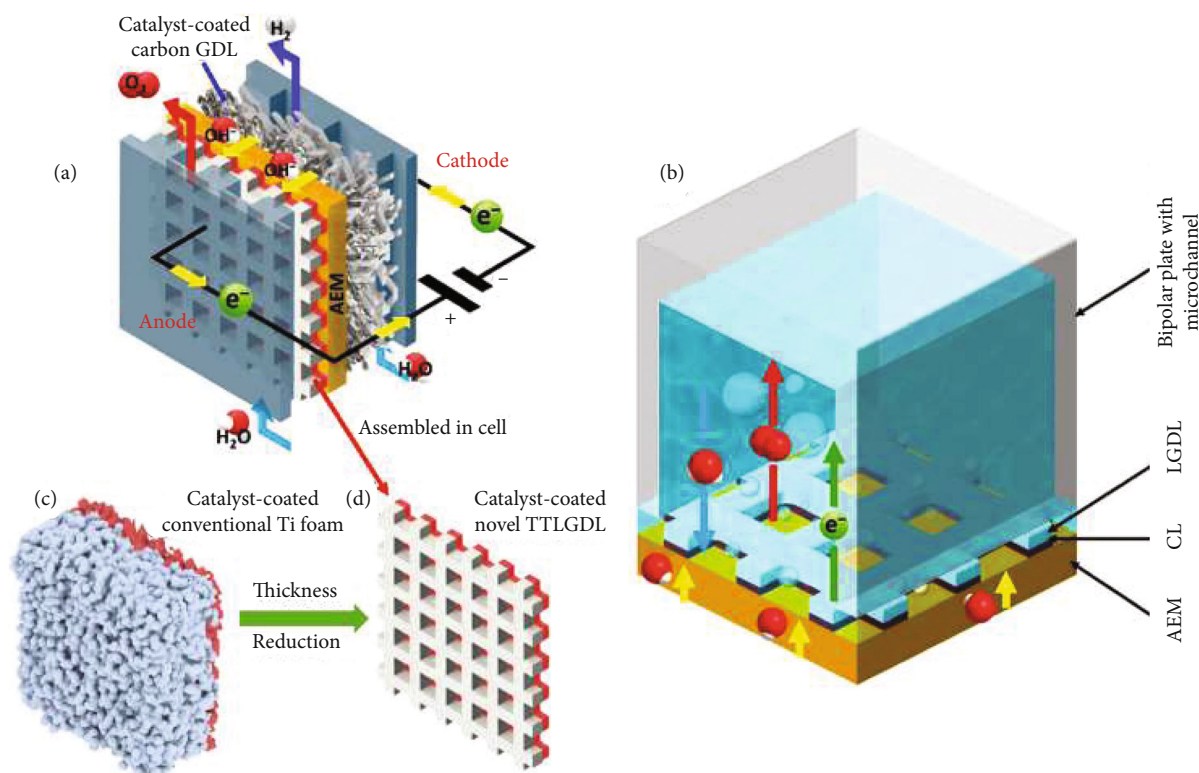
FIGURE 7: (a) Illustration of a traditional MEA for AEMWEs where (b) highlights reactant/product transportation in the anode GDL/MPL/ CL/AEM interface. (c) Conventional anodic three-dimensional foam GDL compared to a (d) two-dimensional titanium grid-style GDL. Reprinted with permission from [51]. Copyright 2023 American Chemical Society.

causing issues with mass transportation at high current densities. This is also seen in the work of Park et al. [31] where the foam outperforms the felt at high current densities in the LSV curves in Figure 4(b) and at low frequencies in the Nyquist plot in Figure 4(c).

However, a similar study produced an opposing conclusion by comparing a gold-coated three-dimensional titanium foam anode GDL against the tuned two-dimensional titanium grid anode GDL shown in Figure 7 [51]. The diffusive efficiency of the latter resulted in a better performance compared to the gold-coated titanium foam, in contrast to the conclusions in [36]. Curiously, this trend persisted even after normalising for iR-contributions, indicating a clear need to optimise the pore sizes and hierarchy in the three-dimensional titanium foam GDL.

Pore size is an important aspect when assessing bubble dynamics, where smaller pore sizes are generally preferred as they yield greater interfacial contact with the MPL and/ or CL. However, smaller pore sizes increase the breakthrough pressure of bubble diffusion [54, 58], implying that a greater pressure is necessary to dispel the evolved gases. This results in greater MT overpotentials caused by increased capillary and bubble pressure, meaning that moderately small pore sizes of 10 to 12 μm are the most suitable [59].

This has also been noted for 3D printed, variable grid-sized nickel GDLs, where oxygen bubble dynamics were investigated using a high-speed camera to assess bubble residency time and escape diameter [48]. Increasing the size of

the anode grid from 40-240 μm lowered the adhesion force between the gas bubbles and the GDL to almost zero, which in turn reduced the bubble residence time/escape diameter. These effects almost eradicated MT issues, resulting in rapid formation and detachment of small bubbles. However, electrical conductivity and catalyst use were also continuously reduced in this range, and increasing the grid size to 440 μm markedly reduced the total cell performance.

The combination of GDL and MPL characteristics was achieved by creating a pore size gradient to enhance fluid flow, as illustrated by vacuum plasma-sprayed anodic Ti-GDLs, where it contributed to lowering tortuosity, capillary pressure, and bubble point [34]. The optimal pore size for the GDL side facing the CL was determined to be between 6 and 11 μm while retaining an overall porosity greater than 22%, thus agreeing with previous research [59]. The adverse effects of reducing the overall GDL pore volume were observed during MEA hot pressing, where the 30% reduction in the secondary pore volume resulted in a 43.2% reduction in current density at 1.80 V [37]. The importance of a porosity gradient has also been determined through modelling, where the supply of reactants was improved by a high porosity near the flow field and the removal of products was optimised by a low porosity near the anode CL [60].

The importance of pore size originates in the process of in-pore bubble removal, a process occurring either by frontal displacement or through bubble snap-off [61]. The former occurs when the electrolyte flushes bubbles up through the pore
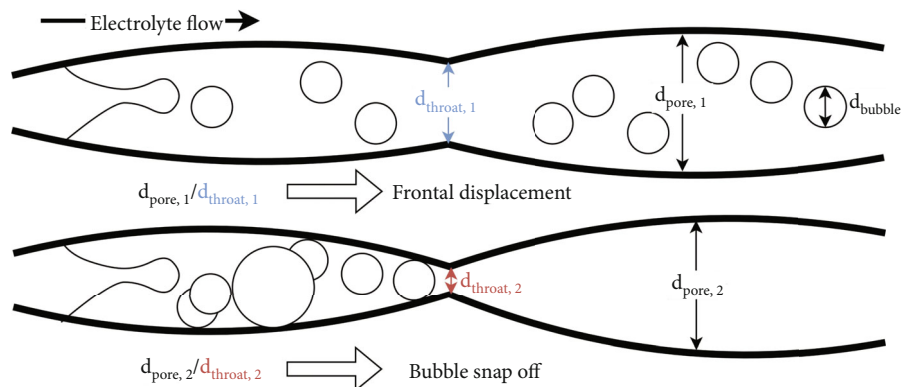
FIGURE 8: GDL pore tunnels illustrating bubble dynamics as a factor of throat and pore diameter.

throats, and the latter when the electrolyte covers the pore walls and forms a cover at the throat of the pore. Snap-off causes bubbles to be trapped within the pores while surrounded by the electrolyte. This is partly why small pore diameters will induce overpotentials [59, 61], as the ratio of frontal displacement to snap-off will be affected by the capillary number and the d_{throat}/d_{pore} ratio as illustrated in Figure 8. Ideally, the ratio of pore throat diameter to bubble diameter should be greater than unity ($d_{pore}/d_{bubble} \geq 1$) to ensure rapid gas transfer under practical current densities. Nanowires, microfiber felts, and foams were compared by Yang et al. [61], where nickel foam was considered the least likely to trap evolved gas considering its great porosity and low d_{throat}/d_{pore} ratio, followed by the nickel microfiber felt and then the nickel nanowire. However, the order was reversed with respect to the electrochemically active surface area (ECSA), nano – wire > microfiber felt > foam. As such, the nickel microfiber felt produced the greatest performance due to the trade-off between a larger ECSA and improved fluid dynamics.

The effect of intelligent pore designs has been shown to reduce mass transportation losses by 76.7%, which was attributed to fast coalescing bubbles that increased the snap-off frequency [62]. These factors were decisive in accelerating product (oxygen gas) removal, thus enabling rapid supply of reactant (electrolyte) to active catalytic sites.

A useful additive to control the wetting behaviour of the GDL is PTFE [32, 33, 63]. Its hydrophobicity helps to accelerate bubble detachment and to control the amount of humidity admitted to the CL, which is most important for cells operating above $1.0 \, A \, cm^{-2}$. Similarly to most additives, the content of PTFE can be optimised where several reports have specified around 9-10 wt.% [32, 33]. The use of PTFE is a trade-off, as it is also a natural insulator and will contribute to the total ohmic resistance of the cell [42].

3. Microporous Layer

The goal of the microporous layer (MPL) is to provide interfacial contact between the GDL and CL in the three-phase interface, supply reactant, remove product, and protect the membrane from perforation by providing mechanical support. Little attention is paid to this layer, despite several studies showing its benefits. Its ideal attributes are com-

monly included by modifying either the GDL [46] or the CL [32, 33]. The benefits were clearly shown in a statistical study in which an MPL was created by adding a carbon layer on top of the GDL [41]. The importance of both the type of GDL and the presence of a carbon layer was highly correlated with the reduced operating voltages. Since the aforementioned study did not specifically include the MPL in their statistical analysis, it is highly likely that the GDL/MPL is the single most important component in the MEA, as opposed to their conclusion of giving this title solely to the GDL.

Similarly to the GDL, porosity is a key aspect in satisfying fluid dynamic requirements. Being closer to the CL, a greater emphasis lies on handling fluids in a gaseous phase, as opposed to both phases equally. Studies of how MPL porosity and pore size affect electrolyser performance confirm several trends from related GDL studies that specify the positive effects of appropriately small pore sizes at the CL-facing interface [49, 59, 61, 64]. A balance of porosity and electrical conductivity is key, as increasing one will reduce the other. Multilayer titanium MPLs with a graded porosity creating appropriate pore sizes reduced MT losses by 45% compared to the commercial single-layer alternative [42, 64]. The advantages of the multilayer design visualised in Figure 9(a) are clear with respect to fluid dynamics, where the gradient lowers the capillary pressure, thus endowing the CL with an ample supply of reactant. The MPL will also be able to handle gas flow if the pore diameter is greater than the bubble departure diameter [57].

Moreover, a smooth MPL surface reduced the activation overpotential by increasing the catalyst utilisation as illustrated in Figure 9(b). MPLs have generally been associated with improved kinetics in the low current density region, which is attributed to improved contact in the MPL/CL/membrane interface [65]. Here, the pore size gradient is shown, which allows the product gases to effectively diffuse away from the CL surface, freeing up additional space for more reactants.

The performance increase experienced by air-plasma-sprayed GDL-MPLs was also attributed to improved porosity and greater pore volume [44]. Optimising the pore volume in the MPL-CL interface contributes to catalyst
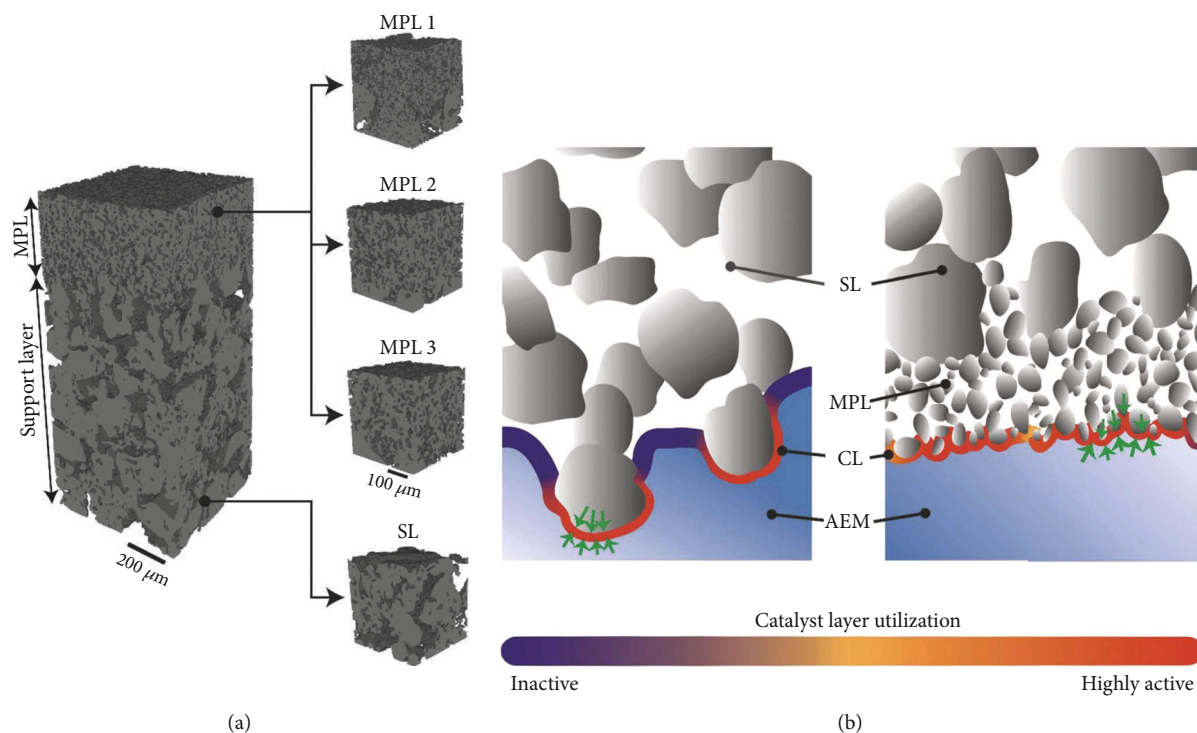
FIGURE 9: (a) Three-dimensional X-ray tomographic microscopy figure of a multilayer GDL with graded MPL porosity over a single layer (SL). (b) The difference in catalyst utilisation with surface roughness. There is a significant increase in catalyst utilisation when employing a smooth surface when the MEA is assembled by laying the GDL/MPL/CL sandwich on top of the membrane. Reprinted with permission from [64]. Copyright 2023 John Wiley and Sons.

utilisation, since MPLs capable of handling two-phase flow will aid in removing gas bubbles and thereby free active areas of the CL. The ideal thickness of an MPL lies in the range of 15-20 μm, where thicker layers may induce MT overpotential due to longer gas diffusion pathways [42]. The porosity of the MPL is important for gas removal around active sites. Modelling efforts have shown that maintaining a low porosity in the anode MPL-CL interface is essential to complete this task while simultaneously retaining a low ICR [60].

Although many choose to address this aspect through a combined GDL-MPL or an MPL-CL, examples have been found in the literature where this aspect has been created separately [41, 63]. The creation of an MPL has been carried out by applying a layer consisting of carbon black (CB) and ionomer [63]. CB is reputed for its expansive specific surface area, a powerful asset when trying to increase interfacial contact [2]. Creating such a layer of both CB and ionomer may result in a conductive layer with great interfacial contact. Common commercial products include carbon-based alternatives with built-in MPLs which are frequently used in the literature, examples of which include Sigracet and Toray [23].

Although the MPL increases interfacial surface contact in the MEA, it is also an additional component which will contribute to the combined series resistance of the cell. Studies utilising an SbSnO$_2$-covered titanium felt MPL on the anode of a PEMWE revealed that while the MPL increased catalytic performance through improved interfacial contact, the additional series resistance was more detrimental to the overall cell performance under practical current densities

[65]. However, exchanging the tested MPL with a more electrically conductive material might ameliorate the issue.

The importance of electrical conductivity goes beyond that of simply reducing the ohmic overpotential, as several other aspects related to the transfer of charge may be enhanced by an intelligent MPL design. Reducing the activation overpotential is also possible by increasing the surface area and altering the roughness of the surface. This will also result in a uniform pressure distribution which improves the use of the catalyst through an improved MPL-catalyst interface [49, 64]. Moreover, such interfaces enable the use of thinner membranes, which contributes to lowering the ohmic overpotential. To this effect, catalyst utilisation was almost trebled in recent work [64] due to a uniform MPL-CL interface.

3.1. GDL-MPL Summary. The importance of the GDL and MPL is clear. Combining the necessary features of both layers into a single component lowers cell complexity and the number of interfaces, which in turn improves the ohmic resistance. The optimal GDL/MPL is usually composed of nickel with a graded porosity where the pore size increases as one moves away from the CL. However, a thin carbon layer may be added to ungraded nickel foam to replicate the MPL. Pore size should never be smaller than the average bubble size. GDL/MPL thickness should mirror gasket thickness to avoid high ohmic/MT overpotential for thick/thin gaskets. Planar MPL surfaces are of the utmost importance for lowering ICR and increasing catalyst utilisation.
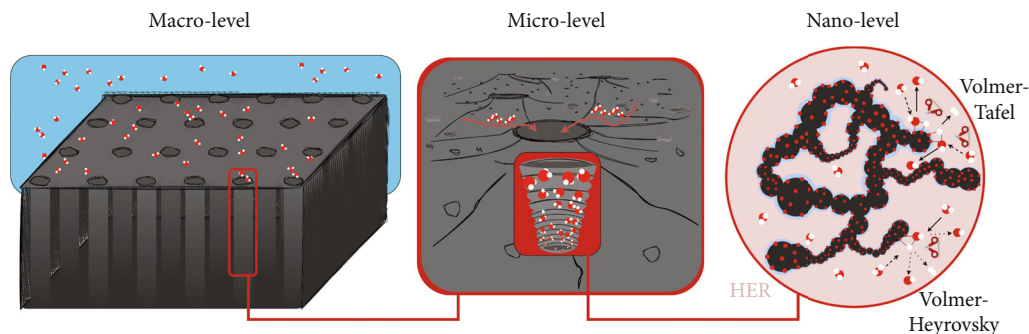
Figure 10: Schematic of the catalyst layer (CL) illustrated on the macro-, micro-, and nanolevel for the hydrogen evolution reaction (HER).

4. Catalyst Layer

The catalyst layer (CL) can be created in many ways, including spray-coating catalytic ink, electrodeposition, and screen printing. Ideal CLs have an extensive, porous surface area, which transports the reactant and the product to and from the many active sites of the electrode. Similarly to all parts of the MEA, CLs also require a delicate balance between a low ICR and effective fluid transport [66]. This is shown in Figure 10, where the macrolevel shows a perfectly flat porous surface providing a low ICR in the GDL/CL interface, while allowing easy access for reactants/products. The microlevel indicates the minor imperfections that comprise a large electrochemically active surface area (ECSA), where the reactants can penetrate the visible CL surface. The nanolevel shows the active sites of the catalyst where the reactant, in this case, water for the hydrogen evolution reactions (HER), can proceed through either the Volmer-Tafel pathway or the Volmer-Heyrovsky pathway.

4.1. Method of Application. The creation of the CL can be facilitated in several different ways, the two most common methods being the catalyst-coated substrate (CCS) and catalyst-coated membrane (CCM). Here, a catalytic ink is applied onto either a substrate or onto the ion-conducting membrane, respectively. Both methods have their advantages over the other, though a general trend is to employ the CCM pathway for creating an efficient AEMWE. The CCM offers great benefits for electrolysers and fuel cells, as the ICR is low because of the intimate contact between CL and the membrane. This method also grants an increased specific surface area, halves the ohmic resistance relative to CCS MEAs, and increases catalyst utilisation [67]. These reasons underline why this is the preferred method for the construction of high-performance electrolysers and fuel cells [36, 67].

The CCS method is the simplest, as one has the liberty of choosing a substrate and subsequently performing additional treatments, which would otherwise have adversely affected the membrane for CCM configurations. While it is possible to perform three-electrode measurements on CCMs, some engineering will be required to correctly place the reference electrode in the AEMWE [49, 68, 69]. However, one can easily use a CCS in three-electrode measure-

ments and directly use the same electrode in an AEMWE without having to recreate the same electrode. As such, the CCS method is frequently employed and is the most widespread method for studying CLs containing novel electrocatalytic materials.

Seeing the benefits of both methods and bearing in mind the individual characteristics of the anode/cathode, investigations into combining the two methods in a single cell have been carried out. Ito et al. [33] examined these effects, and an optimised configuration was created using the CCS technique for the anode and the CCM technique for the cathode. The CCS anode was utilised because of the weak stability of a CCM anode. This was assigned to an adverse interaction between the oxidative electrochemical environment and the CL, likely due to the low chemical and mechanical stability of the AS-4 anion exchange ionomer (Tokuyama).

Although the method of application (CCS/CCM) may vary, the importance of morphology is as important in the CL as in all other layers of the MEA. The pore structure in the CL was systematically varied in a recent publication [40] by varying the spray coating techniques. The creation of a dense catalyst surface was realised by employing several spray-coating steps, in which the electrode-to-nozzle distance was increased and the quantity of ink was simultaneously reduced for each step. A reduction in surface density was achieved by altering these parameters, allowing the pore structure of the CL to be optimised.

Similar effects were achieved during electrodeposition, since the morphology of the CL was systematically varied by proceeding in control current mode and increasing the current density [67]. This resulted in V-CoP CLs with different morphologies, where the CL pore size-to-electrodeposition current ratio displayed a parabola relationship peaking at $16.87\,\mu m \pm 2.09\,\mu m$ at $2.0\,A\,cm^{-2}$. The size of the pores was reduced with further increases in electrodeposition current density, thereby lowering the ECSA and performance. The depth of the pores also increased while changing the pore size, thereby extending the gas diffusion pathway and overall catalyst loading. As such, maximum performance was not achieved with the highest loading.

To this effect, the issue of catalyst loading is not as straightforward as one might think, as a greater loading does not necessarily produce a superior performance. This is due to an increased gas diffusion barrier, as more catalyst also

implies a thicker CL [41, 45, 63, 67, 70, 71]. Various amounts of IrO_2 and 40 wt.% Pt/C were investigated for anodes and cathodes, respectively, revealing an optimal loading of 2 and 0.4 mg_{metal} cm^{-2}, respectively. The thickness of the anodic CL was calculated at 10.11 μm, thus adhering to the 20 μm MPL thickness limit [42].

The detrimental effect of thicker CLs was experienced by Wan et al. [67], where the ordered layers of V-CoP were systematically increased by raising the electrodeposition current. Despite the superior catalyst loading of MEA-3/V-CoP-3 compared to MEA-2/V-CoP-2, its performance was lower in both three-electrode measurements and in a single-cell AEMWE. This was due to a greater pore depth impeding reactant/product transport. This is a greater issue with CLs employing non-PGMs, as the catalytic loading is usually significantly higher compared against those with, e.g., Pt, leading to catalyst loadings exceeding 10 mg_{metal} cm^{-2} [20, 63]. However, this can be ameliorated by exchanging the traditional flat carbon cloth surface for a porous, nonplanar GDL/MPL as shown by Park et al. [36]. The use of porous stainless steel paper increased the micrometre pore volume, which was to great benefit for the overall electrolyser performance due to the significantly increased ECSA. In addition, stainless steel paper anode substrates spray-coated with IrO_2 or NiFe significantly improved catalyst utilisation by ×6 and ×7 when the catalyst loading was changed from 2.0 to 0.2 mg cm^{-2}.

Although the thickness of the CL affects performance, the density of the CL and the distribution of its density relative to the catalyst surface were deemed to have a greater influence on cell performance in a recent study [40]. The greatest performance was achieved with a dense catalyst layer near the surface, thereby corresponding to the findings of earlier GDL/MPL studies on pore gradients. Naturally, the density of the CL was correlated with changes in MT overpotential, and its position relative to the surface was related to activation overpotential. Nevertheless, the transfer of electrons is only one of the halves, with respect to the charge going through the CL, as one must also consider the ionic charge. Here, the anion exchange ionomer is pivotal.

4.2. Ionomer.

An ionomer is a type of polymer, i.e., a long chain of repeating units where other examples include proteins and rubber. Ionomers consist of both ionised and electrically neutral units that are attached to the backbone through covalent bonds. AEM water electrolysers and fuel cells require the ionomer to transport the OH$^-$ charge carrier to/from the membrane from/to the active sites of the catalyst (depending on whether the cathode/anode is considered), while mechanically binding the catalyst layer together to form a pore network in the CL [38, 68, 72]. The ionomer also aids in anchoring the CL as a whole to the underlying substrate, thereby providing mechanical stability and prolonging the longevity of the ECSA. The ideal content of the ionomer is an optimisation issue, as ionomers are ion carriers and possess insufficient conductivity for electrons [72, 73]. Too much ionomer can impede electron transfer, too little, and the hydroxide ions might not reach active catalytic sites.

The choice of ionomer is usually dependent on the type of AEM, as it is advantageous to use similar ion carriers and avoid competing chemical environments [1]. However, utilising a liquid version of the AEM as the ionomer is discouraged due to the different roles of the AEM and ionomer. Specifically, low gas permeability is necessary for an AEM to inhibit oxygen and hydrogen gas crossover, while the ionomer requires high gas permeability to quickly dispel the product gases, thus avoiding blockage of active catalyst sites [74].

Currently, there are several commercially available ionomers, namely, Nafion® (DuPont) [68, 72], Aquivion (Solvay S.A.), Sustainion (DiOxide Materials) [16, 43, 75, 76], Aemion (Ionomr) [76–78], PiperIon (Versogen) [39, 63, 76, 79], Durion [70] and Pention (Xergy), Fumion (FuMA-Tech) [36, 68, 75, 77], and Tokuyama (Tokuyama) [33, 75, 80, 81]. In addition to commercial products, experimental ionomers are also frequently reported [1, 20, 38, 41, 82].

Tokoyama was among the first to provide commercial AEMs and ionomers more than ten years ago [83], although there is little recent use of their products, since the brand has been discontinued. Adverse effects were experienced when the catalyst detached itself from the membrane when the anode was prepared as a CCM, an effect attributed to the poor mechanical/chemical stability of the AS-4 ionomer (Tokuyama) [33]. However, Tokuyama compared favourably with the FAA-3 Fumion ionomer (FuMA-Tech) with respect to swelling effects associated with hydration [75].

In addition to matching the chemistry of the AEM, selecting an ionomer with a high ion exchange capacity (IEC) has been shown to be advantageous for maintaining cathodic humidity while operating with a dry cathode, due to the affiliated increase in water uptake (WU) [84]. The aspect of IEC and WU is also complex, as a pronounced IEC/WU ratio is usually accompanied by excessive swelling, which can compromise the mechanical integrity of the CL by dislodging catalyst particles, lowering the ECSA and increasing the ICR [1, 2, 38].

4.2.1. Anode Ionomer.

Considering the different electrochemical environments of the anode/cathode, and the opposing roles of water as product/reactant therein, the role and impact of the ionomer will change depending on which electrode is considered. The role of water as a product on the anode places great importance on hydrophobicity to avoid MT issues. To this effect, early ionomer optimisation studies utilised small additions of electrically neutral PTFE in anodic CLs to adequately address these problems [32]. The ideal content was quantified to 9 wt.%, enabling the formation of the necessary pore structures without suffering the insulating effects of PTFE which increase the ohmic resistance. Subsequent studies have investigated the range of 1-10 wt.% and confirmed this quantity [33].

The use of the electrically charged Fumion FAA-3 ionomer has been systematically varied in the range of 10-40 wt.% with a NiO catalyst (5 mg_{NiO} cm^{-2}), although little change was revealed with respect to both performance and degree of agglomeration [68]. Opposing results have later come to pass, where a peak OER activity was observed for

15 wt.% of the same Fumion ionomer when investigating the range of 7-25 wt.% together with nickel nanoparticles ($5\,mg_{Ni}\,cm^{-2}$) [85]. This loading was sufficient to impart a low charge transfer resistance and high enough to give good adhesion to the substrate while low enough to avoid swelling issues, which would challenge the mechanical stability of the CL. Subsequently, the ionomer loading was also tested for 5, 10, 20, 30, and 40 wt.% with an IrO_2 catalyst ($2.0\,mg_{Ir}\,cm^{-2}$) with the same Fumion ionomer, revealing a clear peak for 10 wt.% [70]. This loading produced the greatest current measured through LSVs, assisted by a low charge transfer resistance and optimised morphology. Further increases in the ionomer content increased R_{ct} and induced MT problems, as an excessive amount will block active sites and reduce the volume of pores. The Fumion FAA-3 ionomer was varied on both anode/cathode simultaneously, producing the highest current for 20 wt.% with an IrO_2 anode ($2.0\,mg_{Ir}\,cm^{-2}$) and a Pt/C cathode ($0.40\,mg_{Pt}\,cm^{-2}$) [50].

This ionomer has later been compared with Aemion AP1-HNN8 [77], using 7 wt.% ionomer with an Ir black catalyst ($3.5\text{-}3.8\,mg_{Ir}\,cm^{-2}$). Aemion AP1-HNN8 did not measure up to the Fumion FAA-3 ionomer, as it failed to establish a sufficiently intimate CL-membrane interface, which resulted in fewer triple phase boundary points and physical loss of Ir from the anode (from 75 at.% to 13-18 at.%). This shortcoming contributed to the enhancement of the ionic resistance in the catalyst layer which resulted in a ×1.7 increase in the ohmic resistance. The Aemion AP1-HNN8 was systematically varied between 4, 7, 10, and 15 wt.% for an IrO_x anode CL ($1\,mg_{Ir}\,cm^{-2}$), where the peak activity was registered at 4 wt.% [86]. However, the associated stability was lower than that of the anode with 7 wt.%, which produced the highest combined performance. This reiterates Cossar et al. [85], as the ionomer content must be high enough to provide binding and stability, but low enough to avoid kinetic/ohmic/MT losses due to swelling and layer heterogeneity.

Similar trends were also found when Aemion AP1-HNN8 was compared with both Fumion FAA-3 and Nafion® [78]. Evaluating the performance of these three ionomers with a NiFe OER catalyst showed a reduced performance for the alkaline ionomers relative to the Nafion-NiFe combination ($5\,mg_{NiFe}\,cm^{-2}$). The origin was theorised to lie in phenyl group adsorption, which could block active OER sites and/or form an acidic phenol, which would lower the local pH and reduce the pH-dependent electrochemical activity [78, 87]. Furthermore, the transformation from Ni(II) to Ni(III) in NiFe catalysts is beneficial for kinetic improvements, although it was inhibited when combined with Aemion AP1-HNN8 due to these adsorption effects.

Phenyl adsorption on OER catalysts occurs through a cleaving of the C-H bond of the phenyl ring. The degree of phenyl oxidation varies quite significantly with the type of catalyst, as a recent study [87] found that the BTMAOH phenyl group was oxidised to a greater extent with Pt/C and IrO_2 compared against the $La_{0.85}Sr_{0.15}CoO_3$ perovskite, due to a weaker surface interaction. Moreover, a great amount of oxygen in the CL was correlated with a stronger adverse interaction with the ionomer. DFT calculations supported the correlation between phenyl oxidation and the phenyl-on-catalyst adsorption energy, indicating additional benefits in choosing non-PGM catalyst materials for AEMWE applications and elucidating the poor long-term alkaline stability of certain PGM catalyst materials.

Several experimental ionomers have also shown potential, where a quaternised poly(carbazole)-based polymer (poly(9-(6-(trimethylammonium bromide)hexyl) -9H-carbazoleco-1,1,1-trifluoroisopropane, abbreviated as QPC-TMA, was compared with the Fumion FAA-3 ionomer [88]. Similar to other publications, an ionomer loading of 10 wt.% was deemed ideal based on loadings between 5 and 30 wt.%, with a 5 wt.% increment. Tailoring the anode/cathode ionomer relative to the intrinsic water requirements is an established practise for fuel cells [1], though the same method has only recently been used for electrolysers [20]. A slightly hydrophobic (≈80% water uptake) ionomer with a high IEC ($2.80\,mmol\,g^{-1}$) was used for the IrO_2 anode ($2.0\,mg_{Ir}\,cm^{-2}$) in combination with a dry cathode, which had a great effect for the general management of water when using an ionomer loading of 10 wt.% [20].

4.2.2. Cathode Ionomer. Cathodes have an intrinsic need for water in the affiliated reduction process, implying the need for hydrophilic materials with high ionic conductivity. The effect of increasing the contribution of the Tokuyama ionomer from 5 to 10 wt.% produced a 47 mV drop in overpotential when combined with a nickel on $CeO_2\text{-}La_2O_3$/carbon support (Acta 4030) ($2.3\,mg_{Ni/CeO_2-La_2O_3/C}\,cm^{-2}$) [33]. The same loading was also determined as optimal when investigating loadings in the range of 10-40 wt.% for the Fumion FAA-3 ionomer with a Ni/C catalyst [68]. A loading greater than 10 wt.% increased the agglomeration of the catalyst, which reduced the frequency of triple phase boundary points, pore volume, and number of active sites.

A similar study comparing the performance of a Pt/C cathode ($0.40\,mg_{Pt}\,cm^{-2}$) with 10, 20, 30, and 40 wt.% of the Fumion FAA-3 ionomer revealed a clear peak activity for 30 wt.% [70]. The charge transfer resistance gradually decreased until 30 wt.%, though additional increases produced a large R_{ct} increment and the onset of MT overpotential. The arrival of these effects underlines the role of the ionomer as a medium of ionic charge transfer and a creator of morphology in the CL.

The cathode ionomer content of Aemion AP1-HNN8 was tested for 10 and 20 wt.% where the former produced the highest performance [86], although the magnitude of the improvement was not similar to that exhibited by Faid et al. [68] for the Fumion FAA-3 ionomer. This may be related to the comparatively lower performance of the Aemion ionomer [77]; however, it may also be affected by the CL application method, since the CCM method was used by Koch et al. [86] compared against the CCS method [68, 77].

The usage of ionomers is most important during the dry cathode/anhydrous mode of operation, as water is the reactant during alkaline HER. A highly hydrophilic (≈350% water uptake) ionomer with a high IEC ($3.43\,mmol\,g^{-1}$) was used with the Pt/C cathode ($0.50\,mg_{Pt}\,cm^{-2}$), which

harmonises efficiently with a slightly hydrophobic anode ionomer and an AEM with a high water diffusivity rate [20]. The ionomer contents of 10, 20, 25, 30, and 40 wt.% were investigated, revealing a peak at 25 wt.% of the PFBP ionomer. This conspired to produce a peak current density of 7.68 A cm^{-2} at 2.0 V, 1.0 M KOH at 80°C. The high water diffusivity allowed for a constant anode-to-cathode stream of reactants, which produced beneficial conditions to achieve this high AEMWE performance, in both a 1.0 M KOH electrolyte and in the rather harsher deionised water.

Polymers of intrinsic microporosity (PIM) have been investigated as AEMs due to their high reported conductivities ($\sigma > 150$ mS cm^{-1}) and flexible design properties; however, it was theorised that the microporosity might cause high gas diffusion rates, leading to a high probability of gas crossover. As such, PIM might not be suitable for creating AEMs but ideal for ionomers. Trifluoromethyl or cyanide-substituted benzaldehydes polymerised poly(phenyl-alkane) to produce several high-porosity ionomers, both with and without porosity-promoting spirobisindane structures [82]. A total of eight different ionomers were used as both anode and cathode ionomers in different AEMWE cells with a uniform loading of 0.75 mg cm^{-2}, where ionomers with spirobisindane structures produced the greatest performances despite similar IECs. Measuring the ECSAs, the AEMWEs with trifluoromethyl-substituted ionomers revealed larger surface areas compared to those with ionomers substituted with cyanide. This was attributed to the greater free volume afforded by the CF$_3$-substituted ionomers with spirobisindane structures, which optimised the transport of ions, water, and gases in the three-phase interface. Durability was also assessed in 1.0 M NaOH ($j = 1.0$ A cm^{-2}, $T = 80$ °C), where the CF$_3$-substituted ionomer with spirobisindane structures (QP1-CF$_3$-3) did not exhibit significant long-term degradation during the 180-hour stability test. Subsequent LSV curves confirmed near-identical performances to those achieved prior to the stability test. When assessing the results of these stability tests, the ionomer is a component that commonly contributes to failure over time [33, 68]. This places great importance in the stability of the ionomer.

4.2.3. Ionomer Stability.

Anion exchange ionomer (AEI) stability is one of the hottest research topics in both AEM water electrolysers and fuel cells [1, 2, 89]. Topics such as the stability of the ionomer itself in either an alkaline or pH-neutral environment, or its stability in combination with various catalysts in either electrolyte, appear to be inexhaustible, considering the amount of materials created.

Following the trend of studies detailing fundamental mechanisms, the combination of AEIs and platinum has been the subject of numerous studies, where it was determined that platinum is adversely affected by the fairly common charge carrier group quaternary ammonium (QA) [90, 91]. This occurs by inhibiting catalyst activity or by specific/covalent interactions between platinum and QA. The severity of active site blockage increased with the length of the alkyl chain, resulting in the following sequence for select charge carrier groups: tetramethyl < tetraethyl << benzyltrimethyl [91]. Strong interactions between the ben-

zyl group of benzyltrimethylammonium and the electrode surface resulted in it having the most significant effect towards site blockage. Two possible adsorption processes for this interaction were proposed, (1) cation-hydroxide-water coadsorbing onto active sites or (2) adsorption of phenyl groups that blocked further catalytic activity [92].

Since the ionomer is tasked with improving the ionic conductivity between interfaces, it can be instructive to consider the double-layer model, where this approach was used in a study of the interaction between AEIs and various platinum surfaces [90]. To this effect, cyclic voltammetry was performed on Pt-Nafion and Pt-AEI, where the initial potential range was gradually extended from 0.05-0.50 V$_{RHE}$ to -0.10-0.50 V$_{RHE}$. The initial range produced customary peaks originating from the desorption of hydrogen (under-potential deposited hydrogen H$_{upd}$) on the anodic scan, with no differences between the two material systems. A significant disparity was observed between the two systems when the potential range was extended to HER potentials, as great differences were observed in the peak associated with over-potential deposited hydrogen (H$_{opd}$).

The origin of H$_{opd}$ itself is theorised to originate in either a superposition of the faradaic current from hydrogen oxidation and H$_{upd}$ pseudocapacitive charge or pseudocapacitance from additional monolayers of HER intermediates. Regardless of origin, the disparity in H$_{opd}$ charge between the two systems does not imply a reduced ECSA from the specific adsorption of AEI-originating moieties, but a reduced HER performance due to their proximity.

This indicates that the AEI affects both the inner and outer Helmholtz plane (IHP and OHP), where most AEI moieties are in the OHP. The presence of AEI in both IHP and OHP was also correlated with an earlier study on the methanol oxidation reaction (MOR) [93], where the potential of the oxidising electrode is naturally positive (relative to the potential of zero formal charge (PZFC)), implying that a positively charged QA cation would be repelled. The reduced MOR performance in the presence of AEI moieties was related to the higher effective potential of the OHP (Φ_2), as the electrostatic effects induced by the chemical potential of the AEI will increase Φ_2 as shown in Figure 11(a)). This limits the crucial transport of OH$^-$ to the IHP, which is necessary to remove CO$_{ads.}$, the by-product of the MOR.

Similarly for the HER, the AEI will increase Φ_2 (Figure 11(b)), meaning a greater electrode potential (Φ_M) is necessary to induce the same potential beyond the electrode surface. This works rather directly on the HER, as the electrode solvation shell is also the reactant, which means that the IHP potential Φ_1 will determine the rate constant.

Since hydrogen evolution proceeds at negative potentials, the chemical activity of the AEI at the OHP will reduce the absolute magnitude of Φ_1, thus weakening the electric field on the water at the IHP. This causes a greater percentage of the IHP water reactant/solvent to orient its dipole so that the hydrogen atoms face the AEI and the oxygen atom faces the electrode surface, as shown in Figure 11(b), thus creating the possibility of lowering the activation energy for OH-H bond cleavage.
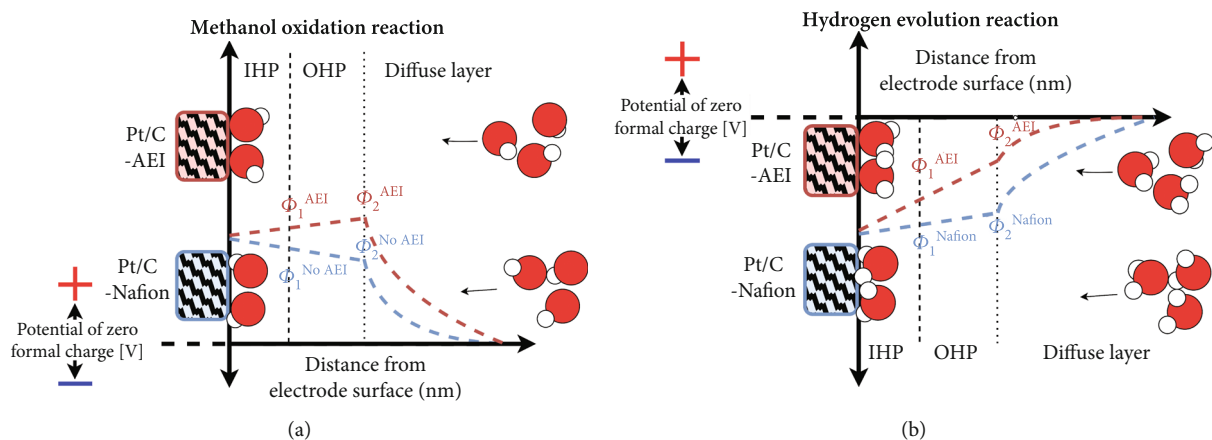
FIGURE 11: The Gouy-Chapman-Stern model of the double layer showcasing the effects of anion exchange ionomers (AEIs) on electrode potentials in the inner and outer Helmholtz plane (IHP/OHP). The chemical potential of the AEI is illustrated in conjunction with the (a) methanol oxidation reaction and (b) the hydrogen evolution reaction studied earlier [93]. Adapted with permission from [90]. Copyright 2023 American Chemical Society.

Generally, little work has been done on the associated stability of ionomers under realistic operating conditions ($E \leq 2.0\,V$, $j \geq 1.0\,A\,cm^{-2}$, $T \geq 50^\circ C$) as their stability under considerably milder conditions is still under investigation [94]. Kang et al. [70] report the stability of Fumion FAA-3 and Durion Orion TM1 ionomers under continuous operations at $0.5\,A\,cm^{-2}$ at temperatures of 50-80°C. Although the Orion TM1 ionomer outperformed Fumion FAA-3, significant voltage degradation rates were still reported, specifically 40, 47, 55, and $321\,mV\,h^{-1}$ for temperatures of 50, 60, 70, and 80°C. The setup with FAA-3 ionomer and AEM rapidly increased to 2.3 V over 3.4 hours, thus ending the test. Similar degradation rates were also reported by Park et al. [36] where the FAA-3 ionomer was employed with IrO_2/NiFe anodes together with a Pt/C cathode. The performance of a single-cell AEMWE operated at 70°C at $1.0\,A\,cm^{-2}$ degraded by 22.7 and $16.7\,mV\,h^{-1}$ in a CCM setup and 22.0 and $11.0\,mV\,h^{-1}$ in a CCS setup utilising IrO_2 and NiFe anodes, respectively.

The stability of thin films composed of commercial ionomers Aemion AP1-HNN8-00-X (Ionomr), Sustainion-XA9 (DiOxide Materials), and PiperIon PAP-TP-85 (Versogen) was evaluated using $1.0\,M\,K_2CO_3$/$KHCO_3$ buffer (pH 10), $1.0\,M\,KOH$ (pH 14), or $1.0\,M$ borate buffer (pH 8) as electrolyte solutions [76]. To simplify the analysis, the thin films did not contain catalyst materials.

Aemion AP1-HNN8-00-X was subject to structural reorganisation in all electrolytes, although complete dissolution was experienced in the K_2CO_3/$KHCO_3$ buffer. The degradation of the polymer backbone through a gradual fracturing into soluble fragments was theorised, based on the complete loss of the ionomer during quartz crystal microbalance tests and the emergence of a C 1s peak at a high binding energy. This is possibly due to the location of the charge carrier group, as it lies in the backbone itself, rather than being attached to a side chain of the backbone.

Aemion was predicted to be vulnerable to nucleophilic attack as illustrated in Figure 12(a), where the ring opening

of the benzimidazolium charge-carrying group and the formation of a carboxylate originating from the polymer resulted in the dissolution of the ionomer thin film. This could occur through a charged adjacent electrode that reduces electron density, causing the OH^- charge carrier in the electrolyte to become strongly nucleophilic, which in turn would degrade the Aemion ionomer considering that it is stabilised through a notable degree of methylation. This was supported by attenuated total reflectance (ATR) FTIR spectroscopy analysis, where the emergence of new modes near $753\,cm^{-1}$ affiliated with changes in aromatic compounds indicates a demethylation of the nitrogen atom in the charge carrier group, due to nucleophilic attack. Furthermore, ATR-FTIR also revealed a reduction in the intensity of the C=N mode, showing the loss of N^+, which was also indicated in the XPS results.

Sustainion revealed greater stability in the K_2CO_3/$KHCO_3$ buffer, which was theorised to originate in the inherent differences in the carbonate/bicarbonate ionic conductivity of the two ionomers. The ionomer was able to rapidly conduct the anions, thereby avoiding the formation of a pH or concentration gradient in the ionomer/electrode interface. However, while the ionomer backbone remained intact as indicated by the thin film remaining on the electrode, the stability of the charge-carrying group was challenged.

Ring opening of the imidazolium charge carrier group is promoted by nucleophilic attack, as illustrated in Figure 12(b), where the reduction in the total C-N/C ratio determined by XPS indicates the loss of the side chains ending in the imidazolium group. This was also supported by the ATR-FTIR spectrum, which exhibits changes in the C=N mode. The loss of side chains was likely preceded by a restructuring of the imidazolium group based on the N 1s spectrum which revealed changes in its oxidation state. The opening of the ring could be a transition stage to side chain loss, or both paths 1 and 2 in Figure 12(b) could occur simultaneously through a nucleophilic attack. An important point is that the Sustainion ionomer did not clearly degrade
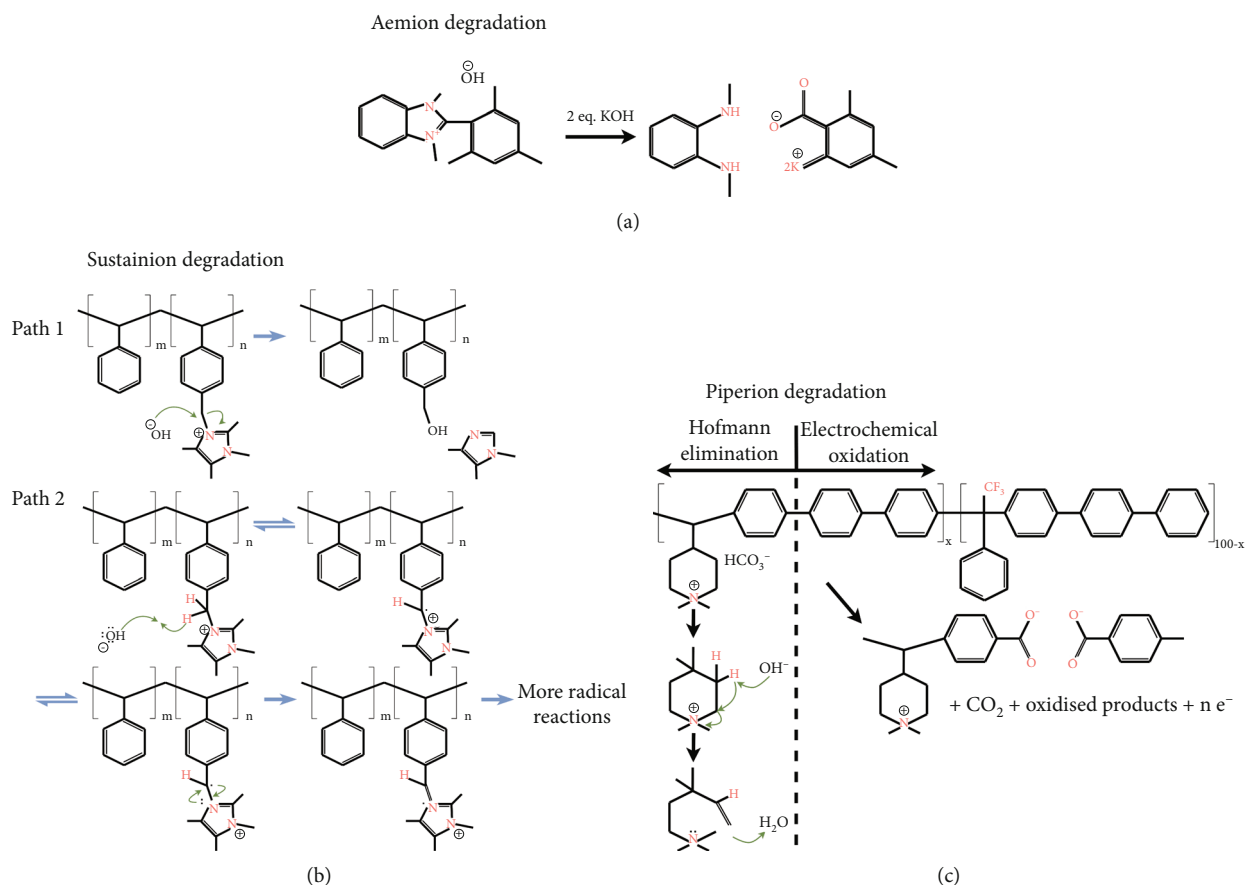
FIGURE 12: (a) Aemion was theorised to experience degradation through nucleophilic displacement or nucleophilic attack on the benzimidazolium C_2 position resulting in the ring opening. (b) Sustainion was also likely affected by imidazolium ring opening, but it could have received a nucleophilic attack on the α-carbon that connects the charge carrier imidazolium and the phenyl group. (c) PiperIon was likely impaired by Hofman β-elimination and S_N2-methyl substitution in the piperidinium ring. Electrochemical degradation (exhibited only for the PiperIon here) is a possibility for all ionomers through highly reactive OER intermediates (HO, HO_2, O_2^-) or generally through other electrochemical reactions under anodic conditions. Adapted with permission from [76]. Copyright 2023 American Chemical Society.

without an applied potential, thereby showing that the nucleophilic attack must be exacerbated by the oxidising potential. Furthermore, OER intermediates such as O_2^-, HO_2, and HO could have oxidised the phenyl group that connects imidazolium to the ionomer backbone, resulting in loss of conductivity.

PiperIon was vulnerable to the $K_2CO_3/KHCO_3$ buffer, similarly to Aemion. The low conductivity of the CO_3^{2-}/HCO_3^- anions might induce electrochemical oxidation of the ionomer, or it may be adversely affected by a lower local pH created by concentration or pH gradients at the thin film/electrolyte interface. Electrochemical oxidation would likely affect the phenyl group connecting the charge carrier and the polymer backbone; however, this degradation was difficult to support as the degradation products may have dissolved. PiperIon has been shown to be subject to considerable oxidation when operated with IrO_2 in pure water AEMWEs [94]. Here, the quantity of XPS-determined C-N bonds was greatly reduced, which was confirmed with a nonexistent N 1s spectrum. Moreover, the F 1s spectrum was decimated, revealing a loss of the trifluoromethyl group.

Density functional theory (DFT) calculations were performed to establish the redox potentials of the three ionomers: Sustainion $(2.18\,eV_{SHE}$ cis, $2.33\,eV_{SHE}$ trans$) >$ PiperIon $(1.78\,eV_{SHE}) >$ Aemion $(1.46\,eV_{SHE})$. Sustainion is affected by competing effects related to π-stacking, specifically a destabilised ground state and stabilisation of the spin density through a multicenter single-electron bond.

Aemion was assumed to be exposed to oxidation considering the low redox potential. Specifically, the nitrogen atom in the benzimidazolium without the attached methyl group was the most vulnerable point, as the methyl group adds spin stabilisation. As such, electrochemical polarisation-assisted ring opening of the benzimidazolium charge carrier group was assumed to be the main degradation method for the Aemion AP1-HNN8-00-X ionomer as shown in Figure 12(c). This could occur through a nucleophilic (OH^-) attack on the polarised ionomer structure, or direct oxidation due to OER intermediates and/or the electrode surface. For Sustainion, protection provided by the charge carrier stabilises the adjacent phenyl ring, rendering the other phenyl ring without imidazolium proximity a more likely target for oxidation. However, the redox potential is

high, and the experimental evidence indicates changes to the nitrogen bonding environment, which would not be the case in phenyl oxidation. With this in mind, oxidation of the C-C bond connecting the phenyl group to the charge carrier group, causing side chain loss, might be the most likely method of degradation.

The activity and stability are aspects that vary from system to system when the catalyst and ionomer are combined, ultimately creating endless combinations. As such, discovering reliable trends will have a great impact in reducing the amount of work necessary to create stable ionomers for AEM electrolyser applications. The stability of the commercial ionomer PiperIon PAP-TP-85 was recently investigated again, this time together with a series of transition metal oxides, and measured against IrO_2 [39]. Catalysts with high electronic conductivity were found to produce higher degradation rates. Both Co_3O_4 and IrO_2 as the most conductive materials maintained degradation rates at 1.8 and 2.6 mV h^{-1} in deionised water for 20 hours ($j = 1.0$ A cm^{-2}, $T = 57°C$). However, the greatest source of degradation was associated with catalyst reconstruction, where iterative dissolution and redeposition altered the ionomer-catalyst interaction and blocked active sites. Due to issues with catalyst-ionomer interactions, several studies have chosen to omit the use of ionomers in favour of creating CLs directly in the GDL itself [71, 95]. Several MEAs without ionomers were tested in a single-cell AEMWE where the peak stability was registered as 0.91 mV h^{-1} after 120 hours in 1.0 M KOH ($j = 0.4$ A cm^{-2}, $T = 40°C$) [71]. Although presenting a fairly low degradation rate, operating conditions were below that which is necessary to compete with established PEM- and traditional AWE-based technologies. Furthermore, the operating voltage ($\approx$2.20 V) is somewhat higher than that shown by other setups that have elected to employ ionomers, indicating that further improvements are possible with including such ion-conducting components in the CL.

The stability and ion-conductive properties of polynorbornenes have been frequently reported for AEMFCs [1, 2], though only recently for AEMWE ionomers [38]. A new experimental ionomer was recently reported, which covalently bonded catalyst, AEM, GDL, and the nonionomeric epoxy binder, to great effect for improving stability. Although stability was initially improved by increasing the amount of the nonionomeric binder, it was only enhanced because the chemical bond of the binder rooted the catalyst and ionomer in place. Moreover, while encased in a binder, the ionomer was unable to bond to the catalyst and AEM, thereby decreasing the ionic conductivity in the MEA and reducing its stability. The novel TP2 ionomer comprised substituent chains (-CH$_2$-CH$_2$-COOH substituent) of notable length that allowed greater flexibility to form covalent bonds between the ionomer and the epoxy binder, thus increasing the ionic conductivity in the CL. The stability of the ionomer was demonstrated by 500 hours of AEMWE operation at 1.0 A cm^{-2}, 60°C in 0.1 M NaOH with no observable degradation. An increase in performance was observed by comparing steady-state LSV curves, an aspect associated with the extended break-in period of the NiFe$_2$O$_4$ anode catalyst.

In contrast to commercial poly(aryl(piperidinium)) (PAP) ionomers with aryl-aryl backbones, experimental ionomers employing polynorbornene ionomers with alkyl-alkyl backbones have shown significantly greater stability [38, 41]. Optimised AEMWEs with such ionomers reported an overall degradation rate of 8.3 μV h^{-1} [41]. Different piperidinium ionomers (poly(fluorenyl-co-aryl piperidinium) (PFAP)) have shown good stability over 1000 hours ($j = 0.5$ A cm^{-2}, $T = 80°C$), where ^{1}H nuclear magnetic resonance revealed an intact backbone and charge carrier group [20]. Similarly, trifluoromethyl-substituted benzaldehyde-polymerised poly(phenyl-alkane) ionomers did not exhibit significant degradation after 180 h in 1.0 M NaOH ($j = 1.0$ A cm^{-2}, $T = 80°C$). The cyanide-substituted benzaldehydes polymerised poly(phenyl-alkane) ionomer, on the other hand, showed irrecoverable loss after 120 h, whereupon the cell voltage suddenly increased from 1.75 to 1.85 over the remaining 60 h of the stability test [82].

4.3. Dry Cathode Operation. Several papers report the benefits from operating an AEMWE without any electrolyte feed to the cathode, in other words, operating with a dry/anhydrous cathode [20, 33, 63, 84, 96]. This implies that the cathodic fluid flow is predominantly gaseous, which enables a simplified MEA design as opposed to that required by a traditional two-phase flow when the electrolyte is supplied to both anode and cathode. In this case, most of the cathodic liquid goes towards maintaining cathodic hydration and HER, which enables the cathode GDL to be replaced with an MPL to enhance catalyst utilisation and lower the ICR and series resistance. This mode of operation creates conditions that are generally quite similar to those experienced in a PEM/AEM fuel cell, thereby allowing the fuel cell know-how to easily be transferred to the electrolyser realm.

This method of operation is possible on the basis of anode-to-cathode water diffusion, which can be easily realised by electing an AEM with a high water diffusivity rate. However, intrinsic effects such as osmotic drag transporting water back to the anode can cause the AEM on the cathode side and the cathode itself to dry out, resulting in elevated ohmic resistance and greater activation overpotential [81, 84]. Accordingly, tailored ionomers are beneficial, where Chen et al. [20] revealed the great potential of placing ionomers with high and low water uptake characteristics on the cathode and the anode, respectively. This resulted in a PGM-AEMWE producing a high performance in 1.0 M KOH ($E = 2.0$ V, $j \approx 7.68$ A cm^{-2}, $T = 80°C$).

Dry cathode operations were visualised in situ through neutron imaging [84], where high IEC ionomers helped to ameliorate adverse effects related to cathode drying. However, the overpotential of mass transport was still observed at high current densities ($\approx$1.5 A cm^{-2}) even with such ionomers in the CL. Removal of the catholyte is therefore possible through the use of high IEC ionomers; however, practical current densities ($j \geq 1.0$ A cm^{-2}) still induce challenges.

Generally, the use of a dry cathode has been shown to be beneficial to the electrolyser performance, as the hydrogen

gas was dryer and of greater purity, while the excess of mass transport overpotential was generally reduced [63, 84, 96]. This is positive because cathodic mass transportation reductions are more noticeable because the cathode gas production rate is stoichiometrically twice that of the anode. There are reports noting negative effects from this operating method at high current densities [81], although this appears to be ameliorated by AEMs with a fair water diffusivity rate that can adequately serve the cathode with enough water through the diffusion from the anode. Long-term performance of the dry cathode AEMWE under practical parameters ($E \leq 2.0$ V, $j \approx 1.0$ A cm^{-2}, $T \geq 50°C$) suffered due to a smaller solvation shell caused by the dry cathode [81, 84]. Increased series resistances were also noted for dry cathodes as a result of the lack of hydration in the AEM, although the use of an ionomer with a high IEC was beneficial for reducing this effect. While the use of an AEM with a high water diffusivity rate was found to be beneficial in reducing these issues, the long-term implications of these aspects remain unreported [63].

4.4. Nonionomeric Binders. While ionomers act as pathways to transfer ionic charge and mechanically stabilise the CL microstructure, it is often the case that additional mechanical support is necessary. Here, nonionomeric binders represent an additional ingredient in the CL, which greatly enhances CL stability by providing mechanical support and protection against chemical attack [96, 97]. Although there are several types of binder available [42], the most widely used type is undoubtedly polytetrafluoroethylene (PTFE), available as powder or suspension [96]. The ideal content has been determined in several publications, where some claim 9 wt.% [32] and some claim 20 wt.% [96].

Most articles use PTFE as their nonionomeric binder; however, bis-(phenol)-A-diglycidyl ether (BPADGE) epoxy adhesive (JB Weld 8265S) dissolved in acetone and combined with an epoxy hardener dissolved in isopropanol has also shown promise [38]. This was shown by utilising a tape test method (ANSI T569~900 J m^{-2}) where adhesive tape was pressed onto the catalyst surface of the electrodes and removed to test the mechanical stability of the CCS. Few particles were on the tape after the use of this nonionomeric binder.

The use of binders can be highly necessary to maintain the ECSA, on which the catalyst is secured. There is a humongous variety of these catalyst materials, for both the anode and cathode. These will briefly be summarised here, and additional information on this specific topic may be found in the following targeted reviews [98–103].

4.5. Anode Catalyst Materials. The anodic oxygen evolution reaction (OER) has found the spotlight in many research papers since the early twentieth century, due to its comparatively feeble electrochemical activity compared to, for example, the acidic hydrogen evolution reaction (HER). This is most aptly depicted by comparing their exchange current densities (ECDs), i.e., their intrinsic activity during a zero net current density. The ECD for the OER and HER under acidic conditions was estimated to 1×10^{-4} mA cm^{-2} and

1 mA cm^{-2}, respectively [104, 105]. The advent of PEM technology in the 1960s caused this topic to gain more traction, as these ECDs represented serious kinetic boundaries that limit the efficiency of PEM electrolysers and fuel cells [2].

The tables turn under alkaline conditions, as the same OER catalysts that are prone to rapid corrosion and dissolution under acidic conditions have been shown to be active and stable in basic electrolytes [1, 101]. Furthermore, the difference in ECD between the alkaline OER and the HER is less severe than under acidic conditions, meaning that research efforts have been more evenly applied between the two reactions when studied in a basic electrolyte.

Novel alkaline OER catalysts are almost exclusively non-PGM, with a steady increase in reducing the use of critical raw materials (CRMs) to decrease CRM dependency as elements such as cobalt and vanadium face increasing scarcity through use in, e.g., the production of batteries/consumer electronics. However, the materials most commonly researched as alkaline OER catalyst materials include iron, nickel, cobalt, manganese, and chromium, usually bimetallic or ternary combinations [1, 2, 106]. One or more of the aforementioned elements are usually combined in spinels, perovskites, and general oxides which have exhibited both activity and stability under alkaline conditions.

NiFe catalyst materials are among the most commonly reported for the OER, where, e.g., 3D-NiFe-LDH films created through a hydrothermal method on nickel foam displayed fair activity [107]. This was explained through an in situ conversion of LDHs to NiOOH, the former of which constituted the OER-active phase. The stability was tested through chronopotentiometry under ambient conditions, and it retained 97.8% of its activity during the 10-hour test (-3.30 mV h^{-1}). This was attributed to the strong catalyst-substrate binding, where even ultrasonic treatment failed to dislodge the catalyst film. While NiOOH may be the active phase during OER for NiFe catalyst materials, the incorporation of Fe has been found to be vital for OER activity [108]. The activity of chemically reduced Ni$_{100-x}$Fe$_x$/50 wt.% CeO$_2$ ($x = 0, 5, 10, 20, 40$ at.%) peaked for Ni$_{80}$Fe$_{20}$/50 wt.% CeO$_2$ due to Fe fusion into NiOOH species. Further increments in Fe content produced segregated Fe-rich phases of lower activity. Details into the activity of NiFe catalysts were also investigated by Tang et al. [109], where nanometer-sized NiFe LDHs in a nitrogen-doped graphene framework (NGF) displayed potential towards the alkaline OER. NiOOH was also determined as the origin to OER activity, which became clear through a comparison of the oxidising peak of the Ni(II)/Ni(III) redox couple and the corresponding LSV curves. Stability was ascertained through 3.3 hours of chronopotentiometry at around 15 mA cm^{-2}, where a degradation rate of 3.57 mV h^{-1} was determined based off the LSV curves measured before and after. While a peak in activity has been determined in NiFe layered double hydroxides (LDHs) with 20-25 at.% of Fe [108, 110, 111], the associated stability has been questioned [106, 112]. Incorporating a greater at.% of Fe was affiliated with increased stability, where a decent stability was displayed despite the rigorous square wave potential cycling [106]. A different Ni-Fe LDH material revealed an outstanding activity and durability

where the at.% of Fe was close to 50% [112]. The Ni-Fe LDH electrode was created through corroding an Fe substrate in a Ni salt solution, producing a NiFe LDH thin film which retained its activity and durability over 5000 hours at 1.0 A cm^{-2}. The outstanding durability was attributed to the stable LDHs which acted as both protective film over the Fe substrate and an active catalyst layer. Similarly to NiFe catalysts, the Fe content was varied in several $W_xCo_yFe_{1-x-y}$/NF catalysts to create $W_{0.5}Co_{0.4}Fe_{0.1}$/NF which displayed activity and stability towards the OER [113]. The addition of Fe lowered the degree of Co oxidation and thereby optimised the OER intermediate binding energies, thus enhancing OER kinetics. The 504 hours of stability shown through chronopotentiometry at 20 mA cm^{-2} was likely assisted by the presence of Fe, inhibiting the typical stability issues associated with Co oxidation. The use of heteroatoms such as B, S, N, and P as dopants to modify the electronic structure of transition metals has also shown promise in recent years [101, 114], as exemplified by a Ni_2Fe_8-Ni_2S_3/NF catalyst [13]. The Ni_2Fe_8-Ni_2S_3/NF catalyst performed admirably in retaining relevant current densities ($j \geq 1.0$ A cm^{-2}) for 300 hours with little degradation. Post-stability XPS and XRD reveals the S leached out from the surface oxide layer but remains stable within the material, enabling the material to maintain both activity and stability. Other transition metals may also be used in conjunction with LDHs, where CoFeCe$^{0.5}$ were developed to great effect [115]. The interface between the CoFe LDHs and the CeO$_2$ enhanced OER activity by altering the rate-determining step (RDS) through lowering the OH$^-$ adsorption energy, leading to more facile OER kinetics. The use of multi-interface materials for lowering energetic barriers associated with a RDS is a well-known method in creating catalyst materials for composite reactions [13, 101, 114, 115]. To that effect, a V-doped CoCO$_x$ on nickel foam (NF) was synthesised and displayed activity towards both the evolution of oxygen (OER) and hydrogen (HER) in alkaline electrolytes [116]. The V-doping altered the electronic structure of the CoCO by shifting the d-band closer towards the Fermi level, resulting in a significant increment in activity towards the OER. Another example involving V and Co elected to add P, resulting in a most efficient catalyst material towards both the OER and the HER [67]. A series of V-CoP catalysts were developed, differentiated by the current density employed during the electrodeposition process. All had the same intrinsic OER activity (η@ 20 mA cm^{-2}), showing that the electrodeposition current density aided in regulating mass transport characteristics. The highly porous structure afforded by the high current density electrodeposition process allowed the electrode to efficiently handle large currents during oxygen evolution, resulting in rapid bubble detachment from the many active sites. The comparatively high degradation rate seen in some works [107, 109] may be related to the short time frames in which stability was measured. Similar catalyst materials based off NiFe LDHs [117] show comparable performances.

Table 2 shows a largely representative overview of the catalyst materials for the alkaline OER, which is mainly composed of various nickel-iron combinations. Stability is

mostly tested in an alkaline electrolyte; however, there is an increasing focus on increasing catalyst activity in deionised water. This matches the imperative of alkaline water electrolysis with deionised water as an electrolyte, whereupon achieving a respectable performance ($E \leq 2.0$ V, $j \geq 1.0$ A cm^{-2}, $T \geq 50°$C) with non-PGMs will likely make PEM-based water electrolysis obsolete.

Creating a material which displays catalytic activity in an analyte that is initially void of ions is tough, which has in many cases contributed to a redoubling of efforts to create non-CRM catalyst materials for KOH electrolytes instead. Herein, stainless steel is inexpensive and ubiquitously produced for many applications and has recently shown fair OER activity displayed in alkaline electrolytes. From this, a current trend has developed to use stainless steel GDLs as both GDL and OER catalysts [95, 119–121].

The following reviews may be consulted for additional information on alkaline OER [98–100].

4.6. Cathode Catalyst Materials.

The alkaline HER is quite different from its acidic counterpart, where the origin behind the difference in ECD which spans two orders of magnitude has been a research hot spot for several decades [101, 104, 105, 122]. Therefore, the alkaline HER presents several difficulties from an activity point of view, and its low activity is the reason why this reaction receives so much R&D attention.

Similarly to the OER, current R&D efforts on the HER are almost exclusively focused on non-PGMs with an increasing emphasis on non-CRMs to reduce the financial cost associated with catalysts [1]. The grand variety of HER catalyst materials currently being investigated includes alloys and oxides, nitrides, phosphides, chalcogenides, codoped materials and surface-modified varieties thereof [101].

NiMo is a commonly used material towards the alkaline HER, where a magnetic field-assisted growth method was utilised to create NiMo nanowires [123]. The temperature was optimised to 65°C with respect to the ECD, resulting in a material both active and stable towards the alkaline HER. The good activity was attributed to the improved hydrogen adsorption binding energy on Mo through the alloying with Ni. The activity of NiMo was also investigated through the creation of a $MoNi_4/MoO_2$@Ni HER electrode which exhibited a 0 mV onset potential, a low Tafel slope, and fair stability [124]. Here, the $MoNi_4$ nanoparticles were determined as the most active towards the HER, where their intrinsic activity surpassed even that of Pt in 1.0 KOH. This was explained by its ability to cleave the OH-H bond in water, and fairly low hydrogen binding energy for facile H-H recombination. Post-experimental SEM/TEM investigations of the catalyst structure show little change in catalyst structure and morphology, indicating the composite material was most resistant to the 30 hours of constant polarisation. Similarly, one of the most efficient non-PGM catalysts to date is composed of NiMo, where processing the NiMo catalyst in a NH_3/H_2 atmosphere created NiMo-NH_3/H_2 which displayed noteworthy HER activity [11]. Here, the added N through the gaseous ammonia was theorised to increase the HER activity of NiMo, as a NiMoN$_x$ phase

TABLE 2: Activity and stability of catalyst materials for the alkaline oxygen evolution reaction, ranked by their stability.

Material	$\eta_{10\,\text{mA cm}^{-2}}$ (mV)	Tafel slope (mV dec^{-1})	Degradation rate
V-CoP-2 [67]	289	60.4	+6.58 μV h^{-1} (500 h), 0.44 A cm^{-2*}, 25°C, 1 M KOH
Ni-Fe LDH [112]	269	48.3	+3.61 μV h^{-1} (5000 h), 1.0 A cm^{-2}, 25°C, 1 M KOH
W$_{0.5}$Co$_{0.4}$Fe$_{0.1}$/NF [113]	250	32.0	+1.80 μV h^{-1} (504 h), 0.02 A cm^{-2}, 25°C, 1 M KOH
Ni$_2$Fe$_8$-Ni$_2$S$_3$/NF [13]	209	55.3	-42.6 μV h^{-1} (300 h), 1.0 A cm^{-2}, 25°C, 1 M KOH
NiFe-LDH/NF [117]	224	52.8	-170 μV h^{-1} (50 h), 0.13 A cm^{-2*}, 25°C, 1 M KOH
Co$_3$O$_4$@Ni-Fe LDH [118]	215	40.4	-250 μV h^{-1} (80 h), 0.01 A cm^{-2}, 25°C, 1 M NaOH
VCoCO$_x$@NF [116]	240	65.0	-480 μV h^{-1} (25 h), 0.01 A cm^{-2*}, 25°C, 1 M KOH
CoFeCe$^{0.5}$ [115]	329	57.0	-710 μV h^{-1} (24 h), 0.01 A cm^{-2}, 25°C, 1 M KOH
Fe-rich Ni-Fe LDH [106]	214	41.0	-1167 μV h^{-1} (100 h), 0.37 A cm^{-2*}, 25°C, 1 M KOH
Ni$_{80}$Fe$_{20}$ [108]	269	43.0	-2500 μV h^{-1} (10 h), 0.01 A cm^{-2}, 25°C, 1 M KOH
3D-NiFe-LDH film [107]	300	43.0	-3300 μV h^{-1} (10 h), 0.20 A cm^{-2}, 25°C, 1 M KOH
nNiFeLDH/NGF [109]	337	45.0	-3567 μV h^{-1} (3.3 h), 0.015 A cm^{-2*}, 25°C, 0.1 M KOH

*This is an average value. The polarity of the voltage rate indicates whether the performance increased (+) or decreased (-) during the stability test.

was indicated through XRD. This is similar to that mentioned for the OER catalysts, as the use of heteroatom dopants can be equally efficient for creating HER catalyst materials through modification of the local electronic structure [101]. Furthermore, the catalytic stability was shown by the low degradation rate of 9.49 μV h^{-1} after 20 hours of chronopotentiometry at 0.40 a cm^{-2} in a three-electrode setup. Stability was also tested in a full AEMWE at 0.50 A cm^{-2} over 25 hours, thereby exhibiting ex- and in situ stability. Various Co-based materials have also shown promise as HER electrodes, where the previously described VCoCO$_x$@NF [116] and V-CoP-2 [67] exhibited activity towards the OER and the HER. For VCoCO$_x$@NF, the doping of vanadium significantly lowered the hydrogen binding energy, accelerating the recombination of hydrogen to great effect relative to CoCO$_x$. While failing to surpass the Pt benchmark at current densities around 100 mA cm^{-2}, it is clear that the VCoCO$_x$@NF will surpass its benchmark at industrially relevant current densities ($j \geq 1.0$ A cm^{-2}). Similarly to the combination of vanadium and phosphorus in [67], Ni was used as the transitional metal in creation of V-Ni$_2$P/Ni$_{12}$P$_5$ [125]. A decent activity and stability was shown for this material, due to an expansive surface area together with many active sites. The Ni-V bridge sites were determined as the most active through selective catalyst poisoning, thereby underlining the importance of the vanadium doping for achieving a high HER activity. Co-based materials have also shown great promise in multi-interfaced materials such as MoS$_2$/NiCo-LDH, where the already HER-active MoS$_2$ was further enhanced by adding NiCo-LDH which will facilitate the OH-H bond cleavage with greater ease [126]. The improved water dissociation step is seen through a decline in the Tafel slope from 97 to 78 mV dec^{-1}, which was also indicated through a near tenfold decline in charge transfer resistance. As such, transition metals can readily catalyse the HER, where a recent paper describing the formation of defective FeOOH on a Cu-Fe$_3$O$_4$ surface was an efficient strategy for increasing its

HER activity [127]. The FeOOH defects induced oxygen vacancies which modulated the chemical composition and electronic structure of the underlying Cu-Fe$_3$O$_4$ surface, thereby lowering the binding energies for water dissociation and subsequent hydrogen desorption and recombination. Chronoamperometry of Cu-Fe$_3$O$_4$ over 50 hours resulted in a doubling of the current through the formation of these FeOOH defects, signifying how the catalyst can be activated in situ to great effect. Heteroatom dopants with Co-based materials have also shown promise towards the HER as a 3-Co$_3$S$_4$NS/NF electrode has demonstrated [128]. Here, the sulphurisation process increased the activity by effectively improving the hydrogen binding energy due to the electronegativity induced by sulphur. While stability was only tested at 10 mA cm^{-2}, the HER activity at this rate was retained with little loss over 220 hours of chronopotentiometry. Moreover, the stability was also tested in an AEMWE over 12 hours at 0.5 A cm^{-2}. Nitrogen was utilised as the heteroatom dopant through nitridation of commercially available nickel foam, resulting in Ni$_3$N$_{1-x}$ HER electrodes comparable to the Pt benchmark [129]. The use of nitridation modified the Ni surface through the presence of nitrogen vacancies such that both the dissociation of water and the subsequent hydrogen desorption and recombination were facilitated at a higher degree of efficiency. Phosphorous may also be employed in a similar manner in combination with such transitional metals, producing a Fe$_2$P-Co$_2$P on cobalt foam (CF) HER electrode. The stability of the electrode was exhibited through composite chronopotentiometry between 10 and 1000 mA cm^{-2} ($i_{\text{mean}} \approx 536$ mA cm^{-2}) over 300 hours, where the morphology and oxidation state of the material remained stable throughout with a small degradation rate. The good activity and structural stability were attributed to the strongly coupled heterojunction between the Fe$_2$P and Co$_2$P interfaces.

The standard benchmark is usually Pt/C, which has long held the gold standard with respect to activity. This material is not treated with the same regard when it comes to stability as shown in Table 3 [130–132], where recent research has

Table 3: Activity and stability of catalyst materials for the alkaline hydrogen evolution reaction, ranked by their stability.

Material	$\eta_{10\,\text{mA cm}^{-2}}$ (mV)	Tafel slope (mV dec^{-1})	Degradation rate
NiMo-NH$_3$/H$_3$ [11]	11.0	35.0	-9.49 μV h^{-1} (20 h), ≈0.40 A cm^{-2*}
3-Co$_3$S$_4$NS/NF [128]	93.0	55.1	-29.1 μV h^{-1} (220 h), 0.01 A cm^{-2}
Fe$_2$P-Co$_2$P/CF [135]	81.0	56.0	-50.5 μV h^{-1} (300 h), ≈0.54 A cm^{-2*}
Ni$_3$N$_{1-x}$ [129]	55.0	54.0	-94.5 μV h^{-1} (50 h), 0.05 A cm^{-2}
Cu-FeOOH/Fe$_3$O$_4$ [127]	12.0	11.0	-110 μV h^{-1} (50 h), ≈0.09 A cm^{-2}
V-Ni$_2$P/Ni$_{12}$P$_5$ [125]	62.0	63.0	-120 μV h^{-1} (50 h), 0.05 A cm^{-2}
V-CoP-2 [67]	44.4	34.6	-133 μV h^{-1} (500 h), 0.44 A cm^{-2*}
MoS$_2$/NiCo-LDH [126]	78.0	76.0	-200 μV h^{-1} (48 h), 0.05 A cm^{-2}
VCoCO$_x$@NF [116]	93.0	63.0	-380 μV h^{-1} (50 h), 0.01 A cm^{-2}
MoNi$_4$/MoO$_2$@Ni [124]	15.0	30.0	-390 μV h^{-1} (30 h), ≈0.10 A cm^{-2*}
NiMo-65 [123]	17.0	43.0	-430 μV h^{-1} (24 h), ≈0.02 A cm^{-2*}
Platinum standard			
Ti$_3$C$_2$T$_x$@Pt/SWCNT [134]	62.0	78.0	+8.68 μV h^{-1} (800 h), 0.01 A cm^{-2}, 25°C
Pt/C [130]	14.6	51.0	-453 μV h^{-1} (24 h), 0.01 A cm^{-2*}, 25°C,
20 wt.% Pt/C/Cu foam [131]	32.0	65.0	-7899 μV h^{-1} (50 h), 1.00 A cm^{-2*}, 25°C,
20 wt.% Pt/C [132]	23.1	54.2	-15238 μV h^{-1} (5 h), 0.01 A cm^{-2*}, 25°C

*This is an average value. All values were tested at 25°C in a 1.0 M KOH electrolyte.

documented notable degradation of Pt/C in alkaline electrolytes affiliated with weaknesses in the anchoring sites of Pt nanoparticles [97, 133]. As such, stability is the most important aspect when evaluating catalyst prospects for use in AEM electrolysers. While the main focus is applied to improving the performance of non-PGM electrodes, there are also research efforts dedicated towards improving PGM stability. This is demonstrated through the development of Ti$_3$C$_2$T$_x$@Pt on single-walled carbon nanotubes (SWCNTs) [134]. Both Ti$_3$C$_2$T$_x$ and SWCNTs do not display any notable HER activity; however, they add electronic conductivity and stability to aid the immobile, catalytically active Pt nanoparticles.

It is quite clear from comparing Tables 2 and 3 that the current densities at which the HER catalysts are evaluated at are significantly lower than that used during OER catalysis. Similar trends are also present in more targeted reviews [101–103], indicating the need for stable materials to catalyse alkaline HER.

4.6.1. Catalyst Layer Summary. An approximation of the ideal CL is shown in Figure 10, where the flat, porous CL surface comprises an abundance of microscopic imperfections that make up a large ECSA filled with numerous active sites. The composition of the CL is usually less than 20 μm of catalyst (with or without supporting materials, e.g., carbon black), ionomer, and possibly a binder when additional mechanical support is relevant. Ideally, the ionomer should provide an ionic pathway for the hydroxide anions while permitting gas diffusion and mechanically stabilising the catalyst onto the MPL substrate. It should also be hydrophobic/hydrophilic for anode/cathode, respectively, ensuring efficient fluid dynamics for mitigat-

ing MT overpotential. The anode catalyst is typically a binary/ternary transition metal oxide, and the cathode is a binary/ternary transition metal.

5. Assembling the Membrane Electrode Assembly: MEA Preparation

The importance of the materials used in the creation of active and durable MEAs is obvious; however, the preparation, assembly, and subsequent analysis procedures will also affect these aspects. The choice of CCS versus CCM, the method of CL application, hot pressing, or regular assembly, all these variables will impact the degree of interaction between GDL, MPL, CL (catalyst, ionomer, and binder), and AEM, and thereby the triple-phase boundary. Similarly, the membrane electrode assembly can be assembled through a great variety of approaches, ranging from simply laying the individual components on top of each other to more complicated methods involving elevated temperature and pressure.

5.1. Thermal Aspects. Thermal aspects of the MEA assembly include some rather obvious aspects such as hot press, to the less obvious, namely, hot plate conditions during the application of the CL, for both CCMs and CCS configurations. A CL is commonly created by spray coating catalyst ink onto an MPL/substrate/membrane using a handheld airbrush connected to either a gas compressor or a N$_2$-gas line, where this choice will depend on how easily the catalyst is oxidised. Other options include ultrasonic spray coating machines, where the same process is performed automatically while the catalytic ink resides in an ultrasonicated chamber. The effect of these two techniques was compared for the anode CL [36], where the high porosity of the airbrushed CL

improved the utilisation of the catalyst. For both the CCS and the CCM method, the substrate/membrane is usually attached to a hot plate (40-100°C) to accelerate the drying process of the applied catalyst layers. This is usually quite straightforward, although the effect of the hot plate temperature can markedly impact the performance of the catalyst layers. Such investigations have been carried out for acidic PEM conditions, where adverse effects were noted for low (40-60°C) hot plate temperatures, owing to an insufficient catalyst-ionomer connection and a higher series resistance relative to the optimal temperature of 90°C [72]. Moreover, this aspect produced the greatest variability in stability of all investigated conditions, including ionomer loading, concentration of solids in ink, water-to-solvent ratio, ink spray rate, and the aforementioned hot plate temperature.

The hot press is a technique originally used for PEM electrolysers and fuel cells that has gradually been transferred to its alkaline counterpart after the membrane characteristics have evolved to allow its employment without degrading the AEM. The goal of hot pressing is to create an intimate interface between GDL/CL and membrane, or between GDL and CL/membrane, depending upon whether the CCS or CCM technique was employed, respectively. Hot pressing is a technique where the membrane is sandwiched in-between the anode/cathode GDL at an elevated temperature and pressure, effectively melting the parts together, without short circuiting the anode/cathode GDLs. Hot pressing has been extensively used for PEMWEs and PEM fuel cells with great effect; however, the effect of such additional temperature treatments creates uncertainty when MEAs containing novel electrocatalytic materials are being tested.

Hot pressing has been investigated by several studies, where 50°C was deemed the ideal temperature [7, 96] with an applied pressure of 395 psi (27.2 bar) [96] for 1 minute [37]. However, the hot-pressed MEA performance declined relative to that of unpressed MEA due to PTFE agglomeration which blocked active catalytic sites and reduced the pore volume in both the CL and the GDL [37].

Direct MEA fabrication is a technique used to produce MEA for PEMFCs [136] and is highly suited to mass production using a top-down approach. Here, a thin membrane layer is cast directly on top of the CL for both the anode and the cathode, after which these two parts are combined before the membrane has solidified. Subsequently, these parts are combined with a GDL to form a complete MEA, as shown in Figure 13 [67]. The benefits of casting the ion-conducting membrane directly onto the CL are threefold; (1) a great interfacial contact is achieved without any additional pressure which could compromise the mechanical integrity of the AEM; (2) the thickness of the AEM can be reduced without the risk of being punctured by other MEA components; and (3) hot pressing is avoided, thereby limiting additional adverse effects on the catalyst layer from elevated temperature/pressure conditions [67].

Operating a AEMWE with a deionised water feed places even greater emphasis on the CL-AEM interface and utilising the direct fabrication method for creating MEAs for such devices resulted in fair performance improvements relative to the traditional CCS and CCM methods. Specifically, the use of direct fabrication reduced the ohmic resistance of AEMWE by 50.3% and 25.2% relative to that displayed with CCS and CCM MEAs under the same conditions [67].

Similarly to what has been discovered about AEM fuel cells, the use of thin membranes is a way to substantially increase the performance of the electrolyser [1, 67]. This drastically reduces the series resistance of the MEA and accelerates AEM fluid transport.

However, the problem of gas permeability increases quite markedly when the thickness of the AEM is reduced, causing a notable decline in safety as the highest hydrogen concentration allowed in the anode is 2.0 vol.%. This is due to the lower limit for hydrogen-oxygen recombination at 4.0 vol.%, where the flame temperature of 3200 K will easily increase the danger through hot spotting and short circuits.

Moreover, thin membranes are significantly more vulnerable to punctures by other MEA components and general deformations that will reduce the CL-AEM contact area, which underlines several other relevant aspects for direct fabrication of MEAs [67, 136].

5.2. Chemical Aspects. Chemical aspects of assembling an MEA include contributions of several facets already covered. However, these should be emphasised on the basis of the possible outcomes. The application of the ionomer to the catalytic ink can be a possible source of error, as the choice of solvent to dissolve the ionomer has proven to be important, as it affects the catalyst-ionomer interaction [78, 137]. Furthermore, how the ionomer is added to the catalytic ink is highly relevant, as the current density was significantly more stable when the ionomer was added directly to the catalytic ink compared to being dropped or sprayed on top of the CL [78]. The impact of the solvent-to-water ratio in the catalytic ink was investigated, where a high water content primarily produced increments in the series resistance [72]. This was associated with changes in the MEA morphology, as the drying time increased with the water content, leading to a heterogeneous catalyst distribution, because of ink pooling. The pooling effect produced segregation between the individual components of the ink, where catalyst particles aggregated into lumps, similar to the process of flocculation. Similar effects were also noted by varying the ink pump rate, where high rates resulted in pooling, and low rates revealed slight impacts from catalyst agglomeration during the coating process.

For preparation before use in an alkaline electrolyte, it is common to soak a CCS in an alkaline electrolyte for at least one hour prior to cell assembly, which is commonly done to exchange the ionomer to hydroxide form [63]. An additional benefit from this includes the hydration of the electrodes, thereby drastically shortening the time it takes for the AEMWE to reach a steady state where the entire MEA is fully soaked in the electrolyte.

Surface area modifications such as acid washing are frequently employed to alter the surface prior to the application of a CL. This usually entails ultrasonicating the GDL or GDL/MPL in, e.g., hydrochloric or sulphuric acid. Although
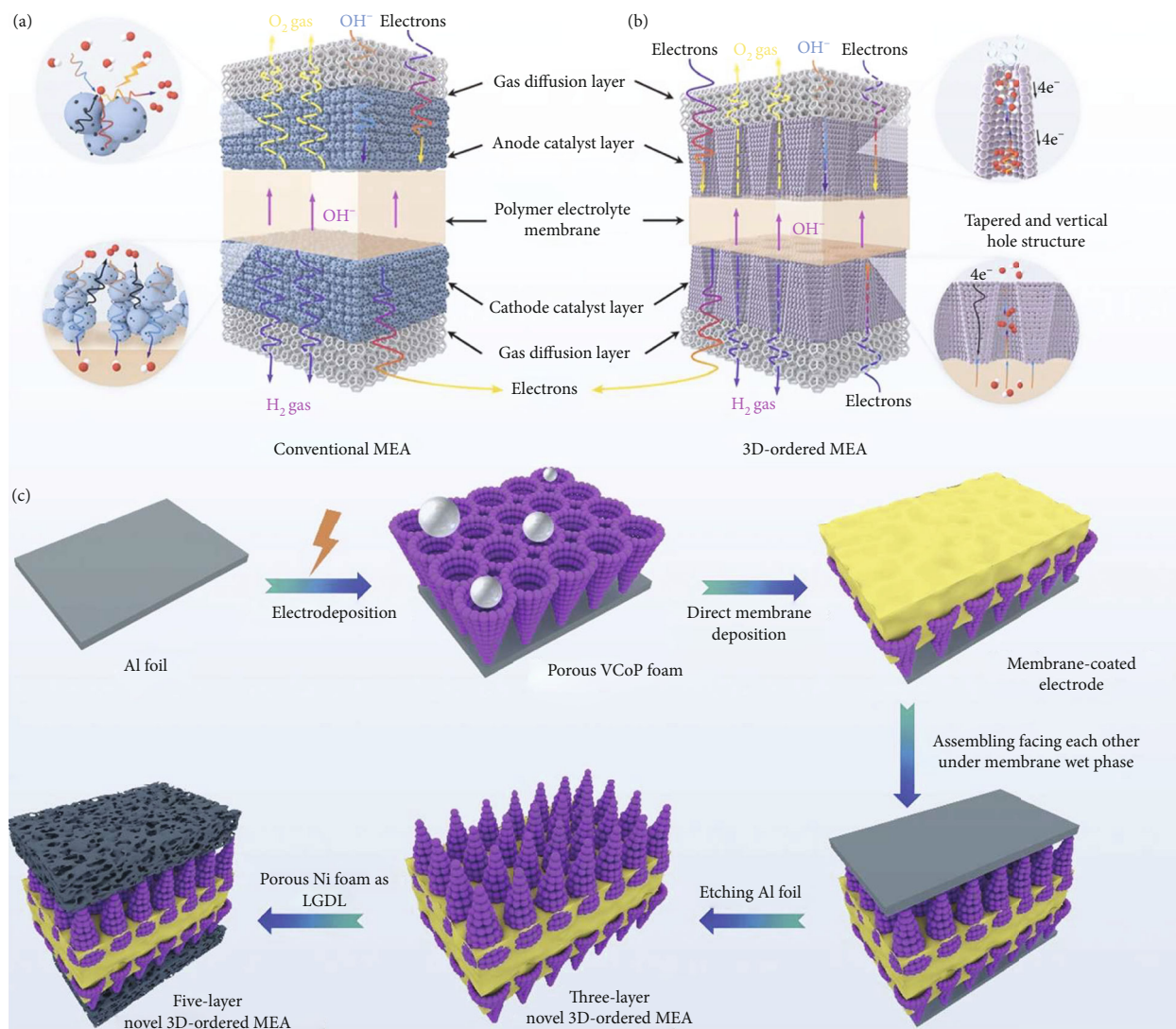
Figure 13: Direct MEA fabrication. Reproduced with permission from the Royal Chemical Society [37].

this can be part of a general cleaning procedure, the ECSA can be notably improved by increasing the acid concentration or the ultrasonication time. The effect of the two acids was compared in a recent study [138] where 15 minutes of ultrasonication in 0.50 M H_2SO_4 was deemed the optimal acid and acid concentration based on reductions in series resistance and increased ECSA shown through charge transfer resistance. The utility of acid-washing nickel foam electrodes is also present after spray coating a CL, as acid-washed, catalyst-coated electrodes display greater ECSAs [43]. This increase is associated with controlled pitting corrosion of the nickel foam surface, producing a more rugged and uneven surface. This was also beneficial for CL stability, as the CL was securely anchored to the many holding points on the GDL created after surface treatment.

5.3. Mechanical Aspects. All individual parts are created, and the cell or stack is ready to be assembled. Here, a myriad of options remain, the outcome of which can still have a great effect on the resulting performance.

All things matter when it comes to optimising cell performance, even tightening the screws. A torque wrench is necessary to control the applied pressure on the cell and ensure a uniform distribution thereof. Moreover, the application of the torque should be applied in a fair way, specifically by tightening each screw in small increments in a star formation [63]. This is most important to avoid puncturing the AEM and generally keep all components in place [37, 63].

Keeping all components in place is most important for maintaining a uniform internal pressure distribution [37], as any deviation will result in hot spotting. This effect arises due to an uneven pressure distribution, which lowers contact resistance at specific points, causing an exponential increase in the local current density. This will result in accelerated ageing of the MEA and eventually a short circuit, as the high local current density will burn a hole in the membrane.

The internal pressure can be increased by altering the thickness of the MEA components relative to the liquid-insulating gaskets. This will improve catalyst utilisation

through a lower ICR, though the overzealous emphasis on this aspect will affect fluid dynamics and exacerbate cathode to anode H_2 permeation [49]. The optimum cell torque was determined to be 4 Nm by Lim et al. [37, 71], where utilising pressure film revealed that this torque produced a uniform pressure distribution and good contact resistance, without impeding mass transportation. The amount of torque applied to the cell screws varies from setup to setup, where various publications report values of 1 Nm [45, 139], 3 Nm [38], 4.0-4.5 Nm [37, 41, 63, 71], 5.6 Nm [39], and 6.8 Nm [20]. The necessary amount of cell compression will vary based off the similarity in thickness between the gaskets and the MEA. Compression is necessary to reduce ICR (ohmic overpotential), though overzealous emphasis will increase MT overpotential; thus, several publications report the use of intermediate torque (4.0-4.5 Nm).

6. Conclusion

This review summarised the state of the art for most aspects related to creating membrane electrode assemblies (MEAs) for anion exchange membrane (AEM) water electrolysers (AEMWEs). The components of the MEA have been systematically reviewed, primarily from the perspective of charge transfer and fluid dynamics. Generally, the development of MEAs for use in water electrolysis cells has met a fork in the road, between the continued development of AEMWEs using a supporting KOH electrolyte, or attempting the arduous journey of trying to replicate these results in cells with pure, deionised water.

The emergence of this piece of cutlery in the road does not affect all aspects of the MEA, where the gas diffusion layer and the microporous layer are almost unaffected by the choice of electrolyte. The combined gas diffusion layer (GDL)/microporous layer (MPL) is the most important part of the MEA on the basis of the level of influence this combined part exerts on the total cell performance. Generally, a graded porosity is necessary to (1) provide electrical conductivity from the flow field to the catalyst layer and (2) facilitate an efficient two-phase flow. These aspects are universal in MEA designs for both PEM and AEM electrolysers and are less subject to change with choice of electrolyte.

The composition of catalyst layers usually includes deionised water, solvents, a catalyst, and an ionomer, where the latter two components are most profoundly affected by electrolyte choice and thus have become the recipient of substantial R&D attention. Catalyst materials for the evolution of both oxygen and hydrogen are almost exclusively based off non-platinum group metals (non-PGMs), with an increasing faction focusing on avoiding critical raw materials (CRMs). These catalyst materials are usually bimetallic and trimetallic transition metals (TMs) and TM oxides. Current research concentrates on non-PGM/non-CRM materials for the evolution of oxygen and hydrogen in both 1.0 M KOH and deionised water, though progress has been particularly slow for the latter.

A swift solution to this slow progress may be available through the creation of conductive and tenacious alkaline ionomers that provide alkalinity to the three-phase interface when an AEMWE is operated with deionised water. The creation of such materials is one of the main topics in AEMWE R&D, as their stability is insufficient in both 1.0 M KOH or deionised water. The creation of an alkaline ionomer that can successfully fulfil this task would altogether remove the need for catalyst materials that are active under neutral pH conditions.

Single-component studies on either the GDL/MPL, the catalyst material, or the ionomer unveil their individual strengths and weaknesses; however, it is their behaviour in an AEMWE that is of consequence. As such, individual flaws may be compensated for by engineering the cell to limit their impact. These are the solutions that will ultimately determine the total performance of the cell and the utility of the technology as a whole.

Conflicts of Interest

The authors declare no potential conflict of interests.

Authors' Contributions

Conceptualisation is done by T.B.F. and S.N.S.; methodology is done by T.B.F., S.N.S., P.H.M., M.L.K., and J.V.H.; validation is done by T.B.F., S.N.S., P.H.M., M.L.K., and J.V.H.; formal analysis is done by T.B.F. and S.N.S.; investigation is done by T.B.F. and S.N.S.; resources are done by P.H.M. and J.V.H.; data curation is done by T.B.F.; writing the original draft and preparation are done by T.B.F. and S.N.S.; writing the review and editing are done by T.B.F.; visualisation is done by T.B.F. and S.N.S.; supervision is done by P.H.M., M.L.K., and J.V.H.; project administration is done by P.H.M., M.L.K., and J.V.H. All authors have read and agreed to the published version of the manuscript.

Acknowledgments

References

[1] T. Ferriday and P. Middleton, "Alkaline fuel cell technology - a review," *International Journal of Hydrogen Energy*, vol. 46, no. 35, pp. 18489–18510, 2021.

[2] T. Ferriday and P. Middleton, "4.07- Alkaline fuel cells, theory and applications," in *Comprehensive Renewable Energy*, T. Letcher, Ed., pp. 166–231, Elsevier, Oxford, Second edition, 2022.

[3] D. Santos, C. Sequeira, and J. Figueiredo, "Hydrogen production by alkaline water electrolysis," *Química Nova*, vol. 36, pp. 1176–1193, 2013.

[4] J. Varcoe, P. Atanassov, D. Dekel et al., "Anion-exchange membranes in electrochemical energy systems," *Energy & Environmental Science*, vol. 7, no. 10, pp. 3135–3191, 2014.

[5] D. Li, A. Motz, C. Bae et al., "Durability of anion exchange membrane water electrolyzers," *Energy & Environmental Science*, vol. 14, no. 6, pp. 3393–3419, 2021.

[6] IEA, *The Future of Hydrogen Seizing today's opportunities*, Tech. Rep., IEA, 2019.

[7] M. Carmo, D. L. Fritz, J. Mergel, and D. Stolten, "A comprehensive review on PEM water electrolysis," *International Journal of Hydrogen Energy*, vol. 38, no. 12, pp. 4901–4934, 2013.

[8] S. A. Grigoriev, V. I. Porembskiy, S. V. Korobtsev, V. N. Fateev, F. Auprêtre, and P. Millet, "High-pressure PEM water electrolysis and corresponding safety issues," *International Journal of Hydrogen Energy*, vol. 36, no. 3, pp. 2721–2728, 2011.

[9] P. Trinke, B. Bensmann, and R. Hanke-Rauschenbach, "Current density effect on hydrogen permeation in PEM water electrolyzers," *International Journal of Hydrogen Energy*, vol. 42, no. 21, pp. 14355–14366, 2017.

[10] D. Henkensmeier, M. Najibah, C. Harms, J. Žitka, J. Hnát, and K. Bouzek, "Overview: state-of-the art commercial membranes for anion exchange membrane water electrolysis," *Journal of Electrochemical Energy Conversion and Storage*, vol. 18, no. 2, article 024001, 2021.

[11] P. Chen and X. Hu, "High-efficiency anion exchange membrane water electrolysis employing non-noble metal catalysts," *Advanced Energy Materials*, vol. 10, no. 39, 2020.

[12] J. Kaczur, H. Yang, Z. Liu, S. Sajjad, and R. Masel, "Carbon dioxide and water electrolysis using new alkaline stable anion membranes," *Frontiers in Chemistry*, vol. 6, p. 263, 2018.

[13] G. Ding, H. Lee, Z. Li et al., "Highly efficient and durable anion exchange membrane water electrolyzer enabled by a Fe-Ni$_3$S$_2$ anode catalyst," *Advanced Energy and Sustainability Research*, vol. 4, no. 1, article 2200130, 2023.

[14] S. Siracusano, V. Baglio, N. Van Dijk, L. Merlo, and A. Aricò, "Enhanced performance and durability of low catalyst loading PEM water electrolyser based on a short-side chain perfluorosulfonic ionomer," *Applied Energy*, vol. 192, pp. 477–489, 2017.

[15] C. Pham, D. Escalera-López, K. Mayrhofer, S. Cherevko, and S. Thiele, "Essentials of high performance water electrolyzers–from catalyst layer materials to electrode engineering," *Advanced Energy Materials*, vol. 11, no. 44, article 2101998, 2021.

[16] B. Motealleh, Z. Liu, R. Masel, J. Sculley, Z. Ni, and L. Meroueh, "Next-generation anion exchange membrane water electrolyzers operating for commercially relevant lifetimes," *International Journal of Hydrogen Energy*, vol. 46, no. 5, pp. 3379–3386, 2021.

[17] Y. K. Choe, C. Fujimoto, K. S. Lee et al., "Alkaline stability of benzyl trimethyl ammonium functionalized polyaromatics: a computational and experimental study," *Chemistry of Materials*, vol. 26, no. 19, pp. 5675–5682, 2014.

[18] N. Du, C. Roy, R. Peach, M. Turnbull, S. Thiele, and C. Bock, "Anion-exchange membrane water electrolyzers," *Chemical Reviews*, vol. 122, no. 13, pp. 11830–11895, 2022.

[19] M. Chatenet, B. Pollet, D. Dekel et al., "Water electrolysis: from textbook knowledge to the latest scientific strategies and industrial developments," *Chemical Society Reviews*, vol. 51, no. 11, pp. 4583–4762, 2022.

[20] N. Chen, S. Paek, J. Lee, J. Park, S. Lee, and Y. Lee, "High-performance anion exchange membrane water electrolyzers with a current density of 7.68 a cm−2and a durability of 1000 hours," *Energy & Environmental Science*, vol. 14, no. 12, pp. 6338–6348, 2021.

[21] AFC Energy Plc, "AFC Energy plc - admission to AIM-first day of dealings," 2007. https://www2.trustnet.com/Investments/Article.aspx?id=200704240801013820V.

[22] S. Grigoriev, V. Fateev, D. Bessarabov, and P. Millet, "Current status, research trends, and challenges in water electrolysis science and technology," *International Journal of Hydrogen Energy*, vol. 45, no. 49, pp. 26036–26058, 2020.

[23] M. Jang, S. Yang, M. Park et al., "Efficient and durable anion exchange membrane water electrolysis for a commercially available electrolyzer stack using alkaline electrolyte," *ACS Energy Letters*, vol. 7, no. 8, pp. 2576–2583, 2022.

[24] B. Britton and M. Moreno, "Aemion+® AEM water electrolysis with excellent iridium-free performance and industrially relevant stability in hot, Caustic Electrolyte," in *Electrochemical Society Meeting Abstracts 243. No. 36*, The Electrochemical Society, Inc., 2023.

[25] S. Palmas, J. Rodriguez, L. Mais, M. Mascia, M. Herrando, and A. Vacca, "Anion exchange membrane: a valuable perspective in emerging technologies of low temperature water electrolysis," *Current Opinion in Electrochemistry*, vol. 37, article 101178, 2023.

[26] Q. Feng, G. Liu, B. Wei, Z. Zhang, H. Li, and H. Wang, "A review of proton exchange membrane water electrolysis on degradation mechanisms and mitigation strategies," *Journal of Power Sources*, vol. 366, pp. 33–55, 2017.

[27] M. Suermann, B. Bensmann, and R. Hanke-Rauschenbach, "Degradation of proton exchange membrane (PEM) water electrolysis cells: looking beyond the cell voltage increase," *Journal of the Electrochemical Society*, vol. 166, no. 10, pp. F645–F652, 2019.

[28] N. Kuleshov, V. Kuleshov, S. Dovbysh, S. Grigoriev, S. Kurochkin, and P. Millet, "Development and performances of a 0.5 kW high-pressure alkaline water electrolyser," *International Journal of Hydrogen Energy*, vol. 44, no. 56, pp. 29441–29449, 2019.

[29] C. Karacan, F. Lohmann-Richters, M. Shviro et al., "Fabrication of high performing and durable nickel-based catalyst coated diaphragms for alkaline water electrolyzers," *Journal of the Electrochemical Society*, vol. 169, no. 5, article 054502, 2022.

[30] X. Z. Yuan, N. Shaigan, C. Song et al., "The porous transport layer in proton exchange membrane water electrolysis: perspectives on a complex component," *Sustainable Energy & Fuels*, vol. 6, no. 8, pp. 1824–1853, 2022.

[31] J. Park, H. Choi, S. Kang et al., "Effect of pore structures in nickel-based porous transport layers for high-performance and durable anion-exchange membrane water electrolysis," *International Journal of Energy Research*, vol. 46, no. 12, pp. 16670–16678, 2022.

[32] M. Cho, H. Y. Park, S. Choe et al., "Factors in electrode fabrication for performance enhancement of anion exchange membrane water electrolysis," *Journal of Power Sources*, vol. 347, pp. 283–290, 2017.

[33] H. Ito, N. Miyazaki, S. Sugiyama et al., "Investigations on electrode configurations for anion exchange membrane electrolysis," *Journal of Applied Electrochemistry*, vol. 48, no. 3, pp. 305–316, 2018.

[34] P. Lettenmeier, S. Kolb, N. Sata et al., "Comprehensive investigation of novel pore-graded gas diffusion layers for higher-performance and cost-effective proton exchange membrane electrolyzers," *Energy & Environmental Science*, vol. 10, no. 12, pp. 2521–2533, 2017.

[35] S. Hu, M. Tian, E. Ribeiro, G. Duscher, and D. Mukherjee, "Tandem laser ablation synthesis in solution-galvanic replacement reaction (LASiS-GRR) for the production of PtCo nanoalloys as oxygen reduction electrocatalysts," *Journal of Power Sources*, vol. 306, pp. 413–423, 2016.

[36] J. E. Park, H. E. Bae, M. Karuppannan et al., "Effect of catalyst layer designs for high-performance and durable anion-exchange membrane water electrolysis," *Journal of Industrial and Engineering Chemistry*, vol. 109, pp. 453–460, 2022.

[37] A. Lim, H. J. Kim, D. Henkensmeier et al., "A study on electrode fabrication and operation variables affecting the performance of anion exchange membrane water electrolysis," *Journal of Industrial and Engineering Chemistry*, vol. 76, pp. 410–418, 2019.

[38] M. Chen, M. Mandal, K. Groenhout et al., "Self-adhesive ionomers for durable low-temperature anion exchange membrane electrolysis," *Journal of Power Sources*, vol. 536, article 231495, 2022.

[39] R. Krivina, G. Lindquist, S. Beaudoin et al., "Anode catalysts in anion-exchange-membrane electrolysis without supporting electrolyte: conductivity, dynamics, and ionomer degradation," *Advanced Materials*, vol. 34, no. 35, article e2203033, 2022.

[40] R. Wang, K. Inoguchi, M. Ohashi et al., "Effect of catalyst distribution and structural properties of anode porous transport electrodes on the performance of anion exchange membrane water electrolysis," *International Journal of Hydrogen Energy*, vol. 46, no. 76, pp. 37757–37767, 2021.

[41] N. Hassan, M. Mandal, B. Zulevi, P. Kohl, and W. Mustain, "Understanding and improving anode performance in an alkaline membrane electrolyzer using statistical design of experiments," *Electrochimica Acta*, vol. 409, article 140001, 2022.

[42] H. Rabiee, L. Ge, X. Zhang, S. Hu, M. Li, and Z. Yuan, "Gas diffusion electrodes (GDEs) for electrochemical reduction of carbon dioxide, carbon monoxide, and dinitrogen to value-added products: a review," *Energy & Environmental Science*, vol. 14, no. 4, pp. 1959–2008, 2021.

[43] T. Ferriday, S. Sampathkumar, P. Middleton, J. Van Herle, and M. Kolhe, "How acid washing nickel foam substrates improves the efficiency of the alkaline hydrogen evolution reaction," *Energies*, vol. 16, no. 5, p. 2083, 2023.

[44] F. Razmjooei, T. Morawietz, E. Taghizadeh et al., "Increasing the performance of an anion-exchange membrane electrolyzer operating in pure water with a nickel-based microporous layer," *Joule*, vol. 5, no. 7, pp. 1776–1799, 2021.

[45] B. Chen, P. Mardle, and S. Holdcroft, "Probing the effect of ionomer swelling on the stability of anion exchange membrane water electrolyzers," *Journal of Power Sources*, vol. 550, article 232134, 2022.

[46] J. Lee, T. Schuler, G. Bender et al., "Interfacial engineering via laser ablation for high-performing PEM water electrolysis," *Applied Energy*, vol. 336, article 120853, 2023.

[47] D. Shoesmith and J. Noël, "3.10- Corrosion of titanium and its alloys," in *Shreir's Corrosion Oxford*, B. Cottis, M. Graham, and R. Lindsay, Eds., pp. 2042–2052, Elsevier, 2010.

[48] B. Huang, X. Wang, W. Li et al., "Accelerating gas escape in anion exchange membrane water electrolysis by gas diffusion layers with hierarchical grid gradients," *Angewandte Chemie International Edition*, vol. 135, no. 33, article e202304230, 2023.

[49] Q. Xu, S. Oener, G. Lindquist, H. Jiang, C. Li, and S. Boettcher, "Integrated reference electrodes in anion-exchange-membrane electrolyzers: impact of stainless-steel gas-diffusion layers and internal mechanical pressure," *ACS Energy Letters*, vol. 6, no. 2, pp. 305–312, 2021.

[50] J. Park, S. Kang, S. H. Oh et al., "High-performance anion-exchange membrane water electrolysis," *Electrochimica Acta*, vol. 295, pp. 99–106, 2019.

[51] K. Li, S. Yu, D. Li et al., "Engineered thin diffusion layers for anion-exchange membrane electrolyzer cells with outstanding performance," *ACS Applied Materials & Interfaces*, vol. 13, no. 43, pp. 50957–50964, 2021.

[52] K. Zouhri and S. Y. Lee, "Evaluation and optimization of the alkaline water electrolysis ohmic polarization: exergy study," *International Journal of Hydrogen Energy*, vol. 41, no. 18, pp. 7253–7263, 2016.

[53] X. Cao, N. Zhao, S. Zhang, L. Zhou, Y. Hu, and J. Yun, "Investigation of the hydrogen bubble effect on the overpotential in an alkaline water electrolyzer," *International Journal of Hydrogen Energy*, vol. 49, pp. 47–57, 2024.

[54] Y. Li, Z. Kang, J. Mo et al., "In-situ investigation of bubble dynamics and two-phase flow in proton exchange membrane electrolyzer cells," *International Journal of Hydrogen Energy*, vol. 43, no. 24, pp. 11223–11233, 2018.

[55] S. Yuan, C. Zhao, X. Cai et al., "Bubble evolution and transport in PEM water electrolysis: mechanism, impact, and management," *Progress in Energy and Combustion Science*, vol. 96, p. 101075, 2023.

[56] B. Huang, C. Lei, X. Sun et al., "Improving mass transfer in anion exchange membrane water electrolysis by ordered gas diffusion layer," *International Journal of Hydrogen Energy*, vol. 48, no. 91, pp. 35453–35462, 2023.

[57] R. Iwata, L. Zhang, K. Wilke et al., "Bubble growth and departure modes on wettable/non-wettable porous foams in alkaline water splitting," *Joule*, vol. 5, no. 4, pp. 887–900, 2021.

[58] Q. Xu, L. Zhang, J. Zhang et al., "Anion exchange membrane water electrolyzer: electrode design, lab-scaled testing system and performance evaluation," *Energy Chem*, vol. 4, no. 5, article 100087, 2022.

[59] S. Grigoriev, P. Millet, S. Volobuev, and V. Fateev, "Optimization of porous current collectors for PEM water electrolysers," *International Journal of Hydrogen Energy*, vol. 34, no. 11, pp. 4968–4973, 2009.

[60] S. Paliwal, D. Panda, S. Bhaskaran, N. Vorhauer-Huget, E. Tsotsas, and V. Surasani, "Lattice Boltzmann method to study the wateroxygen distributions in porous transport layer (PTL) of polymer electrolyte membrane (PEM) electrolyser," *International Journal of Hydrogen Energy*, vol. 46, no. 44, pp. 22747–22762, 2021.

[61] F. Yang, M. Kim, M. Brown, and B. Wiley, "Alkaline water electrolysis at 25 A cm−2with a microfibrous flow-through electrode," *Advanced Energy Materials*, vol. 10, no. 25, article 2001174, 2020.

[62] J. Lee, C. Lee, K. Fahy et al., "Accelerating bubble detachment in porous transport layers with patterned through-pores,"

ACS Applied Energy Materials, vol. 3, no. 10, pp. 9676–9684, 2020.

[63] A. Tricker, J. Lee, J. Shin, N. Danilovic, A. Weber, and X. Peng, "Design and operating principles for high-performing anion exchange membrane water electrolyzers," *Journal of Power Sources*, vol. 567, article 232967, 2023.

[64] T. Schuler, J. Ciccone, B. Krentscher et al., "Hierarchically structured porous transport layers for polymer electrolyte water electrolysis," *Advanced Energy Materials*, vol. 10, no. 2, article 1903216, 2020.

[65] J. Polonskỳ, R. Kodỳm, P. Vágner, M. Paidar, B. Bensmann, and K. Bouzek, "Anodic microporous layer for polymer electrolyte membrane water electrolysers," *Journal of Applied Electrochemistry*, vol. 47, no. 10, pp. 1137–1146, 2017.

[66] X. Peng, Z. Taie, J. Liu et al., "Hierarchical electrode design of highly efficient and stable unitized regenerative fuel cells (URFCs) for long-term energy storage," *Energy & Environmental Science*, vol. 13, no. 12, pp. 4872–4881, 2020.

[67] L. Wan, Z. Xu, Q. Xu, P. Wang, and B. Wang, "Overall design of novel 3D-ordered MEA with drastically enhanced mass transport for alkaline electrolyzers," *Energy & Environmental Science*, vol. 15, no. 5, pp. 1882–1892, 2022.

[68] A. Faid, L. Xie, A. Barnett, F. Seland, D. Kirk, and S. Sunde, "Effect of anion exchange ionomer content on electrode performance in AEM water electrolysis," *International Journal of Hydrogen Energy*, vol. 45, no. 53, pp. 28272–28284, 2020.

[69] T. Ferriday, P. Middleton, and M. Kolhe, "Determining the change in performance from replacing a separator with an anion exchange membrane for alkaline water electrolysis," *Journal of Physics: Conference Series*, vol. 2454, no. 1, 2023.

[70] S. Kang, J. Park, G. Jang et al., "High-performance and durable water electrolysis using a highly conductive and stable anion-exchange membrane," *International Journal of Hydrogen Energy*, vol. 47, no. 15, pp. 9115–9126, 2022.

[71] E. López-Fernández, C. Gómez-Sacedón, J. Gil-Rostra et al., "Optimization of anion exchange membrane water electrolyzers using ionomer-free electrodes," *Renewable Energy*, vol. 197, pp. 1183–1191, 2022.

[72] S. Alia, K. Reeves, J. Baxter, and D. Cullen, "The impact of ink and spray variables on catalyst layer properties, electrolyzer performance, and electrolyzer durability," *Journal of the Electrochemical Society*, vol. 167, no. 14, article 144512, 2020.

[73] W. Xu and K. Scott, "The effects of ionomer content on PEM water electrolyser membrane electrode assembly performance," *International Journal of Hydrogen Energy*, vol. 35, no. 21, pp. 12029–12037, 2010.

[74] Y. Yang, P. Li, X. Zheng et al., "Anion-exchange membrane water electrolyzers and fuel cells," *Chemical Society Reviews*, vol. 51, no. 23, pp. 9620–9693, 2022.

[75] S. Alia, *Hydro GEN: low temperature electrolysis*, US Department of Energy, 2021.

[76] R. Krivina, G. Lindquist, M. Yang et al., "Three-electrode study of electrochemical ionomer degradation relevant to anionexchange-membrane water electrolyzers," *ACS Applied Materials & Interfaces*, vol. 14, no. 16, pp. 18261–18274, 2022.

[77] P. Fortin, T. Khoza, X. Cao, S. Martinsen, A. Barnett, and S. Holdcroft, "High-performance alkaline water electrolysis using Aemion™ anion exchange membranes," *Journal of Power Sources*, vol. 451, article 227814, 2020.

[78] E. Cossar, F. Murphy, J. Walia, A. Weck, and E. Baranova, "Role of ionomers in anion exchange membrane water electrolysis: is Aemion the answer for nickel-based anodes?," *ACS Applied Energy Materials*, vol. 5, no. 8, pp. 9938–9951, 2022.

[79] R. Krivina, Y. Ou, Q. Xu, L. Twight, T. Stovall, and S. Boettcher, "Oxygen electrocatalysis on mixed-metal oxides/oxyhydroxides: from fundamentals to membrane electrolyzer technology," *Accounts of Materials Research*, vol. 2, no. 7, pp. 548–558, 2021.

[80] H. Ito, N. Kawaguchi, S. Someya, and T. Munakata, "Pressurized operation of anion exchange membrane water electrolysis," *Electrochimica Acta*, vol. 297, pp. 188–196, 2019.

[81] A. Kiessling, J. Fornaciari, G. Anderson et al., "Influence of supporting electrolyte on hydroxide exchange membrane water electrolysis performance: catholyte," *Journal of the Electrochemical Society*, vol. 169, no. 2, article 024510, 2022.

[82] S. Q. Fu, B. Hu, J. H. Ge et al., "Application of ionized intrinsic microporous poly (phenyl-alkane) s as alkaline ionomers for anion exchange membrane water electrolyzers," *Macromolecules*, vol. 56, no. 15, pp. 6037–6050, 2023.

[83] Y. Leng, G. Chen, A. Mendoza, T. Tighe, M. Hickner, and C. Y. Wang, "Solid-state water electrolysis with an alkaline membrane," *Journal of the American Chemical Society*, vol. 134, no. 22, pp. 9054–9057, 2012.

[84] S. Koch, J. Disch, S. Kilian et al., "Water management in anion-exchange membrane water electrolyzers under dry cathode operation," *RSC Advances*, vol. 12, no. 32, pp. 20778–20784, 2022.

[85] E. Cossar, A. Barnett, F. Seland, R. Safari, G. Botton, and E. Baranova, "Ionomer content optimization in nickel-iron-based anodes with and without ceria for anion exchange membrane water electrolysis," *Journal of Power Sources*, vol. 514, article 230563, 2021.

[86] S. Koch, P. Heizmann, S. Kilian et al., "The effect of ionomer content in catalyst layers in anion-exchange membrane water electrolyzers prepared with reinforced membranes (Aemion +™)," *Journal of Materials Chemistry A*, vol. 9, no. 28, pp. 15744–15754, 2021.

[87] D. Li, I. Matanovic, A. Lee et al., "Phenyl oxidation impacts the durability of alkaline membrane water electrolyzer," *ACS Applied Materials & Interfaces*, vol. 11, no. 10, pp. 9696–9701, 2019.

[88] M. Cha, J. Park, S. Kim et al., "Poly (carbazole)-based anion-conducting materials with high performance and durability for energy conversion devices," *Energy & Environmental Science*, vol. 13, no. 10, pp. 3633–3645, 2020.

[89] A. Faid and S. Sunde, "Anion exchange membrane water electrolysis from catalyst design to the membrane electrode assembly," *Energy Technology*, vol. 10, no. 9, article 2200506, 2022.

[90] M. K. Bates, Q. Jia, N. Ramaswamy, R. J. Allen, and S. Mukerjee, "Composite Ni/NiO-Cr2O3 catalyst for alkaline hydrogen evolution reaction," *The Journal of Physical Chemistry C*, vol. 119, no. 10, pp. 5467–5477, 2015.

[91] I. McCrum, M. Hickner, and M. Janik, "Quaternary ammonium cation specific adsorption on platinum electrodes: a combined experimental and density functional theory study," *Journal of the Electrochemical Society*, vol. 165, no. 2, pp. F114–F121, 2018.

[92] D. Li, H. Chung, S. Maurya, I. Matanovic, and Y. Kim, "Impact of ionomer adsorption on alkaline hydrogen oxidation activity and fuel cell performance," *Current Opinion in Electrochemistry*, vol. 12, pp. 189–195, 2018.

[93] M. Ünlü, D. Abbott, N. Ramaswamy, X. Ren, S. Mukerjee, and P. Kohl, "Analysis of double layer and adsorption effects at the alkaline polymer electrolyte-electrode interface," *Journal of The Electrochemical Society*, vol. 158, no. 11, 2011.

[94] G. Lindquist, S. Oener, R. Krivina et al., "Performance and durability of pure-water-fed anion exchange membrane electrolyzers using baseline materials and operation," *ACS Applied Materials & Interfaces*, vol. 13, no. 44, pp. 51917–51924, 2021.

[95] S. Sampathkumar, T. Ferriday, P. Middleton, and J. Van Herle, "Activation of stainless steel 316L anode for anion exchange membrane water electrolysis," *Electrochemistry Communications*, vol. 146, article 107418, 2023.

[96] M. Cho, H. Y. Park, H. Lee et al., "Alkaline anion exchange membrane water electrolysis: effects of electrolyte feed method and electrode binder content," *Journal of Power Sources*, vol. 382, pp. 22–29, 2018.

[97] T. Ferriday, P. Middleton, M. Kolhe, and J. Van Herle, "Raising the temperature on electrodes for anion exchange membrane electrolysis-activity and stability aspects," *Chemical Engineering Journal Advances*, vol. 16, article 100525, 2023.

[98] M. I. Jamesh and X. Sun, "Recent progress on earth abundant electrocatalysts for oxygen evolution reaction (OER) in alkaline medium to achieve efficient water splitting–a review," *Journal of Power Sources*, vol. 400, pp. 31–68, 2018.

[99] C. Hu, L. Zhang, and J. Gong, "Recent progress made in the mechanism comprehension and design of electrocatalysts for alkaline water splitting," *Energy & Environmental Science*, vol. 12, no. 9, pp. 2620–2645, 2019.

[100] X. Xie, L. Du, L. Yan et al., "Oxygen evolution reaction in alkaline environment: material challenges and solutions," *Advanced Functional Materials*, vol. 32, no. 21, article 2110036, 2022.

[101] T. Ferriday, P. Middleton, and M. Kolhe, "Review of the hydrogen evolution reaction—a basic approach," *Energies*, vol. 14, no. 24, p. 8535, 2021.

[102] Z. Ge, B. Fu, J. Zhao, X. Li, B. Ma, and Y. Chen, "A review of the electrocatalysts on hydrogen evolution reaction with an emphasis on Fe, Co and Ni-based phosphides," *Journal of Materials Science*, vol. 55, pp. 14081–14104, 2020.

[103] N. Khan, G. Rahman, T. Nguyen et al., "Recent development of nanostructured nickel metal-based electrocatalysts for hydrogen evolution reaction: a review," *Topics in Catalysis*, vol. 66, no. 1-4, pp. 149–181, 2023.

[104] T. Schmidt, P. Ross Jr., and N. Markovic, "Temperature dependent surface electrochemistry on Pt single crystals in alkaline electrolytes: Part 2. The hydrogen evolution/oxidation reaction," *Journal of Electroanalytical Chemistry*, vol. 524, pp. 252–260, 2002.

[105] H. Firouzjaie and W. Mustain, "Catalytic advantages, Challenges, and Priorities in Alkaline Membrane Fuel Cells," *Acs Catalysis*, vol. 10, no. 1, pp. 225–234, 2019.

[106] M. Mehdi, B. S. An, H. Kim et al., "Rational design of a stable Fe-rich Ni-Fe layered double hydroxide for the industrially relevant dynamic operation of alkaline water electrolyzers," *Advanced Energy Materials*, vol. 13, no. 25, 2023.

[107] Z. Lu, W. Xu, W. Zhu et al., "Three-dimensional NiFe layered double hydroxide film for high-efficiency oxygen evolution reaction," *Chemical Communications*, vol. 50, no. 49, pp. 6479–6482, 2014.

[108] E. Cossar, K. Agarwal, V. Nguyen, R. Safari, G. Botton, and E. Baranova, "Highly active nickel–iron nanoparticles with and without ceria for the oxygen evolution reaction," *Electrocatalysis*, vol. 12, no. 5, pp. 605–618, 2021.

[109] C. Tang, H. S. Wang, H. F. Wang et al., "Spatially confined hybridization of nanometer-sized NiFe hydroxides into nitrogen-doped graphene frameworks leading to superior oxygen evolution reactivity," *Advanced Materials*, vol. 27, no. 30, pp. 4516–4522, 2015.

[110] X. Li, F. Walsh, and D. Pletcher, "Nickel based electrocatalysts for oxygen evolution in high current density, alkaline water electrolysers," *Physical Chemistry Chemical Physics*, vol. 13, no. 3, pp. 1162–1167, 2011.

[111] D. Friebel, M. Louie, M. Bajdich et al., "Identification of highly active Fe sites in (Ni, Fe) OOH for electrocatalytic water splitting," *Journal of the American Chemical Society*, vol. 137, no. 3, pp. 1305–1313, 2015.

[112] Y. Liu, X. Liang, L. Gu et al., "Corrosion engineering towards efficient oxygen evolution electrodes with stable catalytic activity for over 6000 hours," *Nature Communications*, vol. 9, no. 1, p. 2609, 2018.

[113] Y. Pi, Q. Shao, P. Wang et al., "Trimetallic oxyhydroxide coralloids for efficient oxygen evolution electrocatalysis," *Angewandte Chemie*, vol. 129, no. 16, pp. 4573–4577, 2017.

[114] J. Paraknowitsch and A. Thomas, "Doping carbons beyond nitrogen: an overview of advanced heteroatom doped carbons with boron, sulphur and phosphorus for energy applications," *Energy & Environmental Science*, vol. 6, no. 10, pp. 2839–2855, 2013.

[115] Y. Park, F. Liu, D. Diercks, D. Braaten, B. Liu, and C. Duan, "High-performance anion exchange membrane water electrolyzer enabled by highly active oxygen evolution reaction electrocatalysts: synergistic effect of doping and heterostructure," *Applied Catalysis B: Environmental*, vol. 318, article 121824, 2022.

[116] A. Meena, P. Thangavel, A. Nissimagoudar et al., "Bifunctional oxovanadate doped cobalt carbonate for high-efficient overall water splitting in alkaline-anion-exchange-membrane water-electrolyzer," *Chemical Engineering Journal*, vol. 430, article 132623, 2022.

[117] Z. Li, M. Shao, H. An et al., "Fast electrosynthesis of Fe-containing layered double hydroxide arrays toward highly efficient electrocatalytic oxidation reactions," *Chemical Science*, vol. 6, no. 11, pp. 6624–6631, 2015.

[118] L. Meng, H. Xuan, X. Liang, Y. Li, J. Yang, and P. Han, "Flower-like Co_3O_4@ NiFe-LDH nanosheets enable high-performance bifunctionality towards both electrocatalytic HER and OER in alkaline solution," *Journal of Alloys and Compounds*, vol. 919, article 165877, 2022.

[119] N. Todoroki and T. Wadayama, "Electrochemical stability of stainless-steel-made anode for alkaline water electrolysis: surface catalyst nanostructures and oxygen evolution overpotentials under applying potential cycle loading," *Electrochemistry Communications*, vol. 122, article 106902, 2021.

[120] H. Zamanizadeh, S. Sunde, B. Pollet, and F. Seland, "Tailoring the oxide surface composition of stainless steel for improved

OER performance in alkaline water electrolysis," *Electrochimica Acta*, vol. 424, article 140561, 2022.

[121] H. Zamanizadeh, A. Barnett, S. Sunde, B. Pollet, and F. Seland, "Performance of activated stainless steel and nickel-based anodes in alkaline water electrolyser," *Journal of Power Sources*, vol. 564, article 232828, 2023.

[122] W. Sheng, H. Gasteiger, and Y. Shao-Horn, "Hydrogen oxidation and evolution reaction kinetics on platinum: acid vs alkaline electrolytes," *Journal of The Electrochemical Society*, vol. 157, no. 11, pp. B1529–B1536, 2010.

[123] A. Nairan, P. Zou, C. Liang et al., "NiMo solid solution nanowire array electrodes for highly efficient hydrogen evolution reaction," *Advanced Functional Materials*, vol. 29, no. 44, article 1903747, 2019.

[124] J. Zhang, T. Wang, P. Liu et al., "Efficient hydrogen production on MoNi$_4$ electrocatalysts with fast water dissociation kinetics," *Nature Communications*, vol. 8, no. 1, article 15437, 2017.

[125] T. Zhao, S. Wang, Y. Li et al., "Heterostructured V-doped Ni2P/Ni12P5 electrocatalysts for hydrogen evolution in anion exchange membrane water electrolyzers," *Small*, vol. 18, no. 40, article 2204758, 2022.

[126] J. Hu, C. Zhang, L. Jiang et al., "Nanohybridization of MoS$_2$ with layered double hydroxides efficiently synergizes the hydrogen evolution in alkaline media," *Joule*, vol. 1, no. 2, pp. 383–393, 2017.

[127] C. Yang, W. Zhong, K. Shen et al., "Electrochemically reconstructed Cu-FeOOH/Fe3O4 catalyst for efficient hydrogen evolution in alkaline media," *Advanced Energy Materials*, vol. 12, no. 16, article 2200077, 2022.

[128] Y. Park, J. Lee, M. Jang et al., "Co$_3$S$_4$ nanosheets on Ni foam via electrodeposition with sulfurization as highly active electrocatalysts for anion exchange membrane electrolyzer," *International Journal of Hydrogen Energy*, vol. 45, no. 1, pp. 36–45, 2020.

[129] B. Liu, B. He, H. Q. Peng et al., "Unconventional nickel nitride enriched with nitrogen vacancies as a high-efficiency electrocatalyst for hydrogen evolution," *Advanced Science*, vol. 5, no. 8, article 1800406, 2018.

[130] C. Ray, S. Lee, B. Jin, A. Kundu, J. Park, and S. Jun, "Conceptual design of three-dimensional CoN/Ni3N-coupled nanograsses integrated on N-doped carbon to serve as efficient and robust water splitting electrocatalysts," *Journal of Materials Chemistry A*, vol. 6, no. 10, pp. 4466–4476, 2018.

[131] A. Kumar, V. Q. Bui, J. Lee et al., *Industry-Applicable, Efficient Hydrogen Evolution Reaction through an Interface-Activated Bimetallic Electrode with Seawater Photolysis in Alkaline Media*, ChemRxiv, 2020.

[132] Y. Guo, B. Hou, X. Cui, X. Liu, X. Tong, and N. Yang, "Pt atomic layers boosted hydrogen evolution reaction in non-acidic media," *Advanced Energy Materials*, vol. 12, no. 43, article 2201548, 2022.

[133] C. Lafforgue, F. Maillard, V. Martin, L. Dubau, and M. Chatenet, "Degradation of carbon-supported platinum-group-metal electrocatalysts in alkaline media studied by in situ Fourier transform infrared spectroscopy and identical-location transmission electron microscopy," *ACS Catalysis*, vol. 9, no. 6, pp. 5613–5622, 2019.

[134] C. Cui, R. Cheng, H. Zhang et al., "Ultrastable MXene@ Pt/SWCNTs' nanocatalysts for hydrogen evolution reaction," *Advanced Functional Materials*, vol. 30, no. 47, article 2000693, 2020.

[135] X. Liu, Y. Yao, H. Zhang et al., "In situ-grown cobalt-iron phosphide-based integrated electrode for long-term water splitting under a large current density at the industrial electrolysis temperature," *ACS Sustainable Chemistry & Engineering*, vol. 8, no. 48, pp. 17828–17838, 2020.

[136] M. Breitwieser, M. Klingele, S. Vierrath, R. Zengerle, and S. Thiele, "Tailoring the membrane-electrode Interface in PEM fuel cells: a review and perspective on novel engineering approaches," *Advanced Energy Materials*, vol. 8, no. 4, article 1701257, 2018.

[137] S. Berlinger, B. McCloskey, and A. Weber, "Probing ionomer interactions with electrocatalyst particles in solution," *ACS Energy Letters*, vol. 6, no. 6, pp. 2275–2282, 2021.

[138] T. Ferriday, S. Sampathkumar, P. Middleton, and J. Van Herle, "Investigation of wet-preparation methods of nickel foam for alkaline water electrolysis," *Journal of Physics: Conference Series*, vol. 2430, no. 1, 2023.

[139] B. Chen, A. Biancolli, C. Radford, and S. Holdcroft, "Stainless steel felt as a combined OER electrocatalyst/porous transport layer for investigating anion-exchange membranes in water electrolysis," *ACS Energy Letters*, vol. 8, no. 6, pp. 2661–2667, 2023.